TARGET NORMAL SHEATH ACCELERATION AS A TECHNIQUE FOR MEASURING NUCLEAR CROSS-SECTIONS

By
Andrew Martin
A thesis submitted in partial fulfillment of the
requirements for the degree of

Bachelor of Science

Houghton University

May 2024

Signature of Author……..
Department of Physics
May 3, 2024

……
Dr. Mark Yuly
Professor of Physics
Research Supervisor

……
Dr. Katrina Koehler
Assistant Professor of Physics

TARGET NORMAL SHEATH ACCELERATION AS A TECHNIQUE FOR MEASURING NUCLEAR CROSS-SECTIONS

By
Andrew L. Martin
Submitted to the Department of Physics
on May 3, 2024 in partial fulfillment of the
requirement for the degree of
Bachelor of Science

Abstract

A Multi-Terawatt Laser (MTW) experiment was performed at the Laboratory for Laser Energetics (LLE) to test the feasibility of using Target Normal Sheath Acceleration (TNSA) to measure 0.1 - 10 MeV light-ion cross sections, especially those involving tritium. In this initial experiment using deuterium, laser pulses (~22 J, 7 ps) struck a 0.25 mm^2 deuterated polyethylene (CD_2) target, ejecting TNSA deuterons that hit a ~2 μm thick natural Li target film on a 25 μm thick stainless-steel substrate, causing the $^7Li(d,p)^8Li$ reaction. The Short-Lived Isotope Counting System (SLICS), consisting of the phoswich scintillator, light guide, and photomultiplier, was placed immediately behind the Li target, and a high-speed CAEN Digitizer was used to count the 840 ms half-life beta decay of ^8Li, starting a few milliseconds after the laser shot. The phoswich detector consisted of a fast thin and slow thick scintillator sandwiched together to allow incident particles to be identified by their different rates of energy loss. Incident deuteron energy spectra were measured using time-of-flight (TOF) to a small scintillator in front of the Li target and, for comparison, with a Thompson parabola spectrometer.

Thesis Supervisor: Dr. Mark Yuly
Title: Professor of Physics

This material is based upon work supported by the Department of Energy [National Nuclear Security Administration] University of Rochester "National Inertial Confinement Program" under Award Number(s) DE-NA0004144.

TABLE OF CONTENTS

TABLE OF FIGURES

Chapter 1

HISTORY OF EXPERIMENT

1.1. Introduction to Nuclear Cross-Sections

Nuclear cross-sections are fundamental to understanding the universe, since they are proportional to the probability of a nuclear interaction occurring. Knowing the cross-section allows thermonuclear reaction rates to be determined, which are then used to predict the abundance of isotopes in stars and in Big Bang models in a process called nucleosynthesis. However, very few cross-sections, especially tritium-induced cross-sections, have ever been measured at the low energies relevant to nucleosynthesis. These tritium cross-sections are particularly important because tritium is one of the lightest isotopes, so it is foundational to the formation of other heavier elements.

One challenge in measuring tritium induced cross-sections is that tritium is radioactive, so putting it in an accelerator contaminates the beamline. One of the few accelerator facilities which historically handled tritium was the Los Alamos Three-Stage Van de Graaf facility, later called the Ion Beam Facility (IBF) [1] at Los Alamos National Laboratory. This facility first accelerated tritons in 1965, and was operational until it was vacated in 1994, and fully deactivated in 1999 [2]. Since it was contaminated with tritium and thus unfit for other purposes, it was demolished in 2005 [3]. Currently no operational particle accelerator facilities exist that accelerate tritium.

Additionally, it is difficult to use traditional accelerator experiments to measure such small cross-sections, especially at typical thermonuclear energies which are important in nucleosynthesis. It would take an unrealistic amount of time to count a statistically significant number of reactions through traditional methods, and too much background would build up during the long intervals of time while the experiment was running. However, it may be possible to use advancements in laser technology to perform such experiments by accelerating a large number of ions at once, in facilities already built to handle tritium.

One such is the Laboratory for Laser Energetics (LLE) in Rochester, New York which specializes in laser and optical physics. In the OMEGA 60 target chamber at LLE, high power, short pulse lasers are used to create thermonuclear reactions in a macroscopic target via inertial confinement fusion (ICF), including tritium-induced reactions. Alternatively, with the OMEGA-EP laser at LLE, high power, short pulse lasers are used to accelerate ions including tritium off a target via target normal sheath acceleration (TNSA). The tritium target is kept in a target chamber that is built to handle tritium, and there is no concern of the beamline being contaminated as there is in a traditional particle accelerator. Because of the very short duration of the laser pulse, this facility can produce many tritium-induced reactions relatively simultaneously, and it may be possible to use it to make tritium cross-section measurements.

1.2. Comparison of Nuclear Experiment Methods

To understand why it is difficult to use traditional accelerator experiments to measure these tiny cross-sections, consider a nuclear physics experiment in which a material composed of a certain isotope A is bombarded with particle x, resulting in the nucleus B produced while a particle y flies away to be detected. This is represented with the nuclear reaction notation A(x,y)B. If the product isotope B is radioactive, it will decay into another isotope C and release another particle z (or more). This reaction and subsequent decay is shown in Figure 1.

The constant of proportionality between the rate of decay and the number of decaying nuclei is λ, the decay constant, or

$$-\lambda N = \frac{dN}{dt}, \tag{1}$$

where N is the number of nuclei of the decaying product B and t is time. Equation 1 can be integrated to give the number of B nuclei as a function of time

$$N(t) = N_0 e^{-\lambda t} \tag{2}$$

where N_0 is the initial number of nuclei. The half-life is inversely proportional to the decay constant and is given by $t_{1/2} = \ln 2/\lambda$.

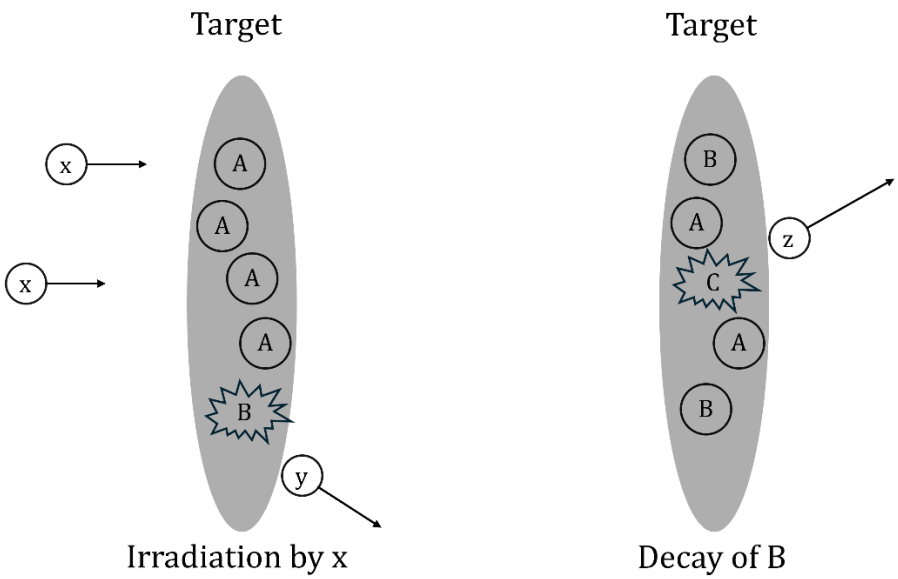

Figure 1. Diagram of A(x,y)B reaction and B decaying. First, a target populated with isotope A is bombarded with particle x, and if the reaction A(x,y)B occurs, then isotope B is produced and particle y is produced. At a later time, after B has been produced in the target, if B is radioactive, it will "z" decay into isotope C and release a particle z.

In a traditional activation experiment, a beam of particles x produced by the accelerator is incident on a target which is made up of the isotope A, and as the reaction A(x,y)B occurs, the target becomes populated with the isotope B as well. However, as nucleus B is being created by A(x,y)B it is also decaying. The rate of B-production in this case is proportional to the number of x particles hitting the target over time, which is the number current F, and the number of A nuclei per area that the beam is incident on, which is the areal density T. So, the rate of change of the number of nuclei B being created is

$$\frac{dN}{dt} = \sigma FT, \tag{3}$$

where σ is the constant of proportionality, called the cross-section. So, the rate of change of the number of nuclei B as they are created and decay is

$$\frac{dN}{dt} = \sigma FT - \lambda N. \tag{4}$$

Integrating this equation yields

$$N(t) = \frac{\sigma F T}{\lambda}\left(1 - e^{-\lambda t}\right). \tag{5}$$

As more product nuclei are created, more decay, so the rate of creation will approach the rate of decay, leading to a limit to the number of nuclei B in the target, as is illustrated in Figure 2. The maximum number of nuclei N_0 present at once occurs when:

$$\frac{dN}{dt} = \sigma F T - \lambda N_0 = 0, \tag{6}$$

so the maximum is

$$N_0 = \frac{\sigma F T}{\lambda}. \tag{7}$$

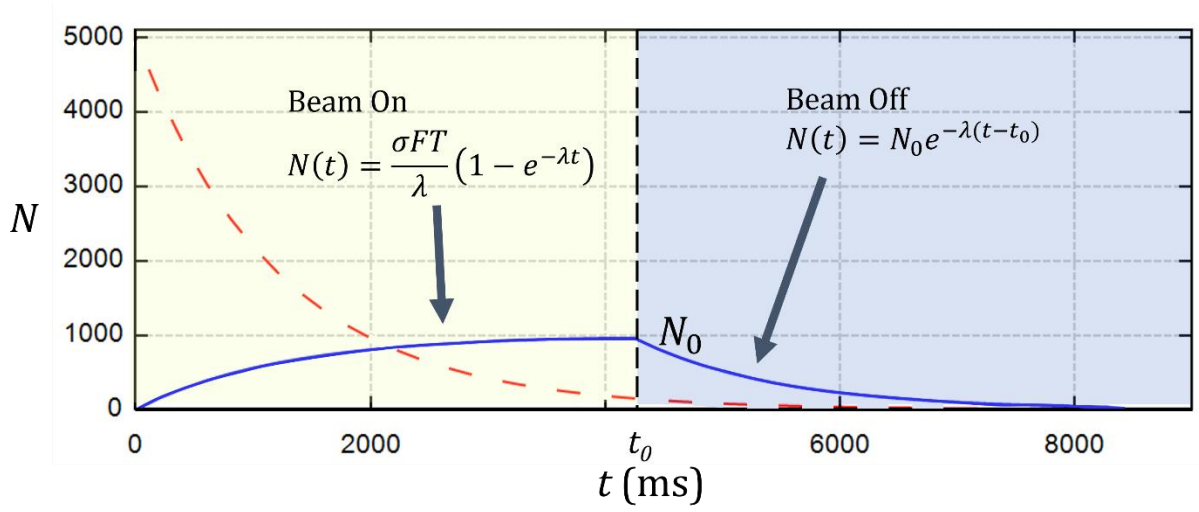

Figure 2. Number of product nuclei over time for accelerator and laser experiments. The solid blue curve represents an accelerator experiment in which product nuclei decay as they are created, so they asymptotically approach a limit N_0. After the time t_0, the accelerator beam is turned off and the radioactive decay curve of that isotope can be measured. The dashed orange curve represents the number of particles over time in an experiment in which all product nuclei are produced at once. This can be done in an experiment in which a laser pulse produces nuclei on a timescale much faster than they decay.

Figure 2, for an example case, shows the number of product nuclei over time for an accelerator experiment and an experiment in which all product nuclei are produced in one burst, as would occur in an experiment using a short pulse laser. In the yellow highlighted

section of time before $t = t_0$ when the accelerator is turned off, the number of product nuclei, N, asymptotically approaches a maximum amount $N_0 = \sigma FT/\lambda$. So, there is a limit to the number of nuclei that can be produced due to the rate of creation of the product nuclei approaching the rate of decay. The beam is turned off at $t=t_0$, and in the blue highlighted section the nuclei decay and are counted. For reactions that have small cross-sections and fast rates of decay, the maximum number of decays that can be counted after the beam is turned off, $N_0 = \sigma FT/\lambda$, is small. The number current (F) can be increased by increasing the beam current, but there is a physical limit to how high beam current can be raised. The areal density (T) can be increased to maximize N_0 as well, but there is also a physical limit as to how thick a target can be made. This process of turning the beam on to build up product nuclei, then turning the beam off and counting can be repeated, but during this process counts from background increase as well, and if there is a significant background count rate relative to actual decays of interest, then the uncertainty in the cross-section measurement becomes large.

To illustrate, consider an experiment in which F foreground counts and B background counts are detected. The number of counts of interest will be $I = F - B$, but since the number of counts is a Poisson distribution, the uncertainty is the square root of the total number of counts, so $\delta I = \sqrt{F + B}$. Imagine the case where the number of background counts is close to the number of foreground count, suppose $F = 100$ and $B = 99$, then $I = 1$ count and $\delta I \approx \sqrt{200}$, so $I \cong 1 \pm 14$. This means the number of background counts must be much less than the number of foreground counts for a statistically significant measurement.

It would be advantageous therefore if the product nuclei were all produced in one burst, so that background would only be counted for a short period. The dashed orange curve on Figure 2 represents an experiment in which the nuclei are produced on a timescale much shorter than their half-life, and so there is no time for them to decay as they are produced. With this method, there is no need to pulse the beam multiple times, so the amount of background is significantly reduced.

Recent advances in laser technology have made this possible. One such technique that could be used to create a large number of product nuclei in one burst is inertial confinement fusion

(ICF). The four stages of ICF are shown in Figure 3. First, high power, short pulse lasers hit the target capsule, heating it isotropically. As material on the outside of the target heats up and blows off, the reaction force from this ablating material compresses and heats the core of the capsule, which creates a dense plasma. In this plasma, nuclei undergo nuclear reactions within a fraction of a nanosecond.

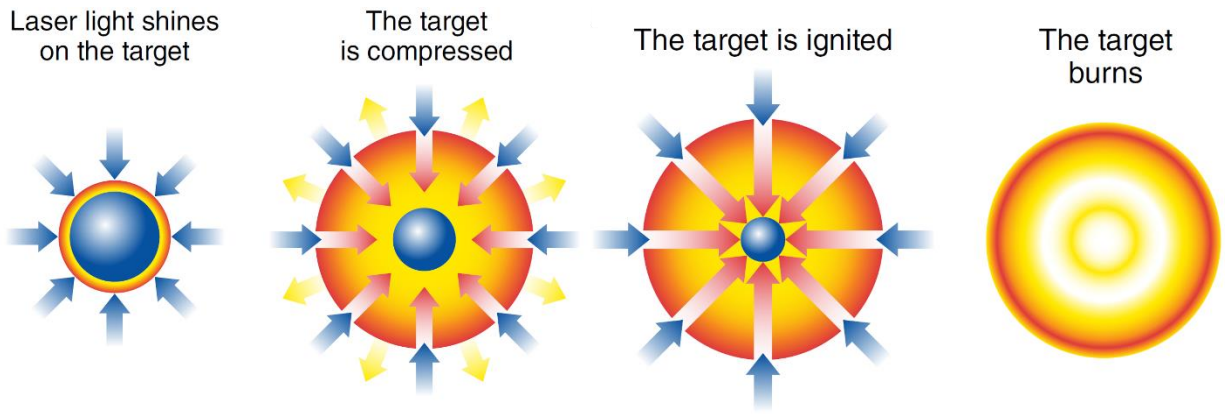

Figure 3. Four stages of ICF. Short-pulse high-power lasers isotropically heat a capsule containing the nuclear fuel of interest. Heat from the lasers causes the outer layer of the capsule to blow off, and the inner material is sent inwards by the reaction force of the ablating material. This sends a pressure shockwave towards the center of the capsule, heating and compressing it to create a plasma in which a macroscopic number of nuclei undergo nuclear reactions within a fraction of a nanosecond. If the target reaches the point of ignition, then the reaction will becoming self-sustaining, and the fusion reactions in the burning plasma will output more energy than was input Figure taken from Ref. [4]

The Short-Lived Isotope Counting System (SLICS) has been developed as a trap, detector, and electronics system to measure low energy light-ion cross-sections of reactions produced in an ICF implosion. ICF is especially useful for tritium reactions, because the OMEGA-60 chamber is built to handle tritium, and with an ICF reaction, a very large number of nuclei are all interacting at once, so even if the cross-section is small, there will be a large yield. Some of the light ions which are fundamental to nucleosynthesis are shown in Figure 4. The isotopes that are highlighted in green can be created through (d,p), (t,p), (d,γ), and (t,γ) reactions. Notice that they all beta decay with half-lives from about 10 ms to 10 s. SLICS was designed to measure isotopes that have these characteristics, since a system that can

measure all of these products would be useful for measuring the cross-sections of many light ion reactions.

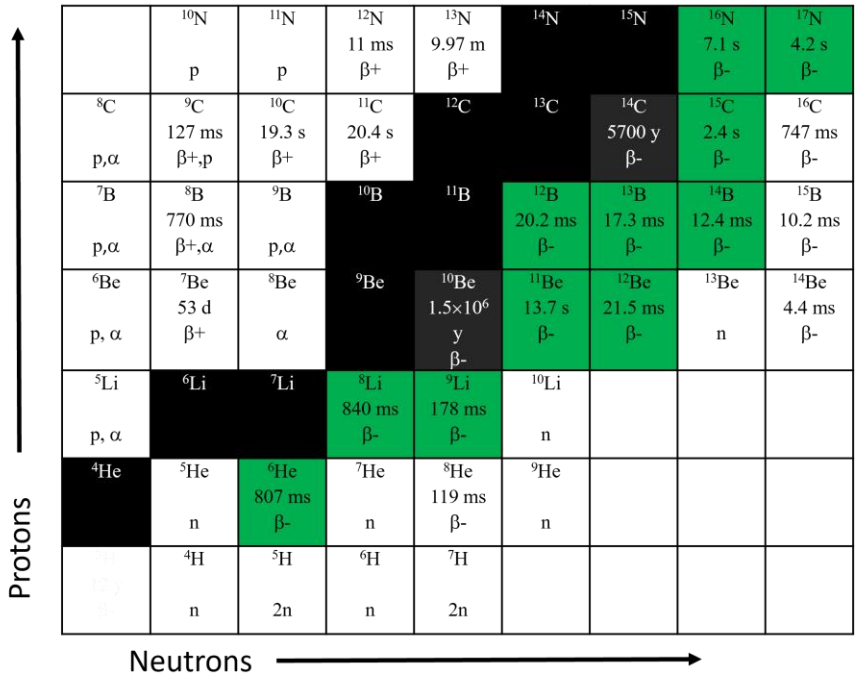

Figure 4. Chart of nuclides. The number of protons in each isotope is on the vertical axis, and the number of neutrons in each isotope is on the horizontal axis. Stable isotopes are highlighted in black. Isotopes in green can be reached through light-ion low energy threshold nuclear reactions. Notice that these isotopes beta decay and have a half-life on the order of 10 ms to 10 s.

Some of the products that could be produced with ICF are shown in Table 1, along with their predicted yield based on the yield of OMEGA shot 77951 which was a tritium-filled SiO_2 capsule "exploding pusher" having a 1.5% - 98.5% DT mixture and reaching an ion temperature of 18.3 keV. These are all light-ion reactions that have little to no data collected for their cross-sections, especially at energies relevant to nucleosynthesis. The first four highlighted reactions have high enough yields that they may be studied at LLE. The green highlighted reactions may be feasible at the National Ignition Facility (NIF), which can produce inertial confinement fusion reactions with 1000 times a higher yield. Since it is possible to produce a significant yield for the first four rows, the two products ^{6}He and ^{8}Li have been the primary focus of preliminary testing experiments.

Table 1. Reactions that can be reached through ICF. The third column is the abundance of the first reactant in the target capsule. The yield is based on the yield of OMEGA shot 77951 which was a tritium-filled SiO_2 capsule "exploding pusher" having a 1.5% - 98.5% DT mixture and reaching an ion temperature of 18.3 keV. Reactivities were calculated using TALYS-1.9 [5] and the S-factor extrapolations of Abramovich et. al. [6]. No cross sections are available for $^{3}H(t,\gamma)^{6}He$ so the predicted yield is based on assuming a branching ratio of 10^{-7}, which is simply an estimated "best case". For $^{11}B(d,p)^{12}B$ and $^{15}N(d,p)^{16}N$ for which data are available at higher energies, TALYS underpredicts the cross sections by as much as a factor of 100.

Reaction	Product Half-life	Reactant Abundance	Predicted Yield
$^{3}H(t,\gamma)^{6}He$	807 ms	^{3}H fill	8×10^{4}
$^{6}Li(t,p)^{8}Li$	840 ms	7.6%	$0.2\text{-}1\times10^{7}$
$^{7}Li(t,\alpha)^{6}He$	807 ms	92.4%	$0.7\text{-}2\times10^{6}$
$^{9}Be(t,\alpha)^{8}Li$	840 ms	100%	5×10^{5}
$^{9}Be(t,\gamma)^{12}B$	20.2 ms	100%	18
$^{10}B(t,p)^{12}B$	20.2 ms	19.9%	5770
$^{11}B(d,p)^{12}B$	20.2 ms	80.1%	534
$^{13}C(t,\gamma)^{16}N$	7.1 s	1.1%	1
$^{13}C(t,\alpha)^{12}B$	20.2 ms	1.1%	677
$^{13}C(t,p)^{15}C$	2.45 s	1.1%	111
$^{14}N(t,p)^{16}N$	7.1 s	99.6%	16
$^{15}N(d,p)^{16}N$	7.1 s	0.4%	0.15

Another method that uses high-power short-pulse lasers to produce a large pulse of ions at once is Target Normal Sheath Acceleration (TNSA). With TNSA, an intense laser pulse accelerates many ions off the surface of a target at once. This target can be doped with deuterons or tritons to produce a deuteron or triton pulse. The concept for this is shown in Figure 5. A high-power, short pulse laser accelerates electrons through a target creating an electric field which accelerates ions from the rear surface of the normal to the surface. The Multiterawatt laser (MTW) at the Laboratory for Laser Energetics is a laser which is capable of TNSA. For an average shot using MTW, about 10^{10} deuterons can be produced in a pulse of 1-10 ps, about 10^{11}-10^{12} times faster than the product nuclei can decay. Only deuterons

can be used in MTW experiments because the MTW chamber is not built to handle tritium, but deuteron-induced reactions and tritium-induced reactions can still create the same reaction products and be used to study similar reactions. For example, the reactions ^{7}Li(d,p)^{8}Li and ^{6}Li(t,p)^{8}Li both produce ^{8}Li. With TNSA, an ion beam [7] is produced on a timescale of 0.1 ns, and the order of magnitude of the half-lives of the decays of interest from Table 1 are 10 ms to 10 s. So, the number of product nuclei will not be limited to $N_0 = \sigma FT/\lambda$ as it would in a particle accelerator experiment.

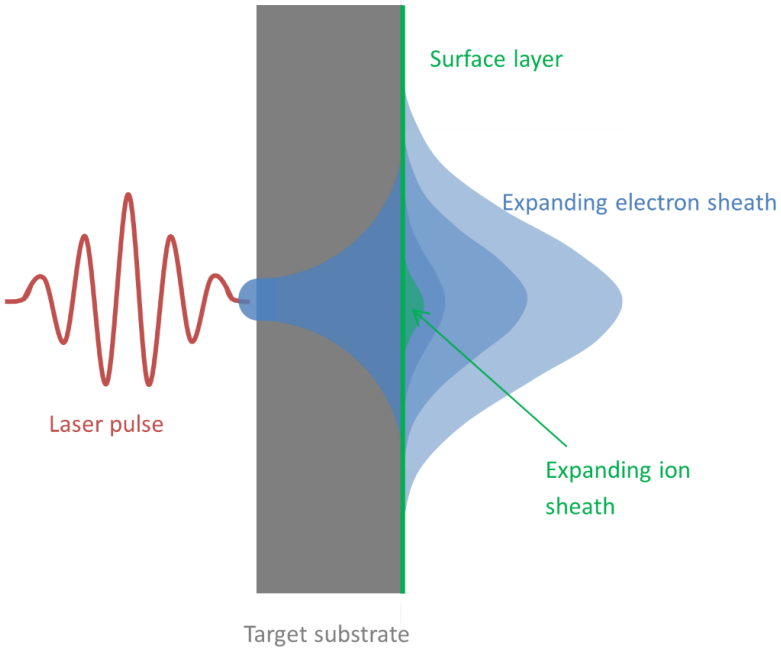

Figure 5. Conceptual diagram of TNSA. A high-power, short pulse laser accelerates electrons through a target. This sheath of accelerated electrons creates an electric field which accelerates ions from the target in the direction normal to the surface. Figure taken from Ref. [7]

1.3. History of Laser Experiments

TNSA has only become possible recently in the history of nuclear physics and lasers, once lasers reached a high enough power. The idea of light amplification by stimulated emission of radiation was first theorized by Einstein in a paper [8] written in 1917. The applications of this technology at the time were unknown, and it would be about 40 years until this technology was first realized in an experiment [9] in 1960, in which a laser was used to excite atoms in a ruby crystal.

A breakthrough in laser technology was the invention [10] of chirped pulse amplification in the 1980s. This technology allows for a much larger power output, about 0.5 TW, which was five times the maximum power output at the time. This increase in power output would eventually lead to the first laser-driven ion acceleration experiment [11] in 1999, in which the VULCAN laser at the Rutherford Appleton Laboratory with intensity $5 \cdot 10^{19}$ W/cm^2 and maximum power output 55 TW was able to accelerate protons with energies up to 18 MeV. Since then, the OMEGA-EP laser [7] at the Laboratory for Laser Energetics (LLE) has been able to produce a triton yield of about 10^{12} using TNSA.

At Houghton, the Short-Lived Isotope Counting System (SLICS) has been developed to measure light ion cross-section using these high power, short pulse lasers. The goal is to take advantage of the properties that laser-driven nuclear activation experiments have over traditional activation experiments, that a large number of nuclei interact without time to decay. So, even for reactions with small cross sections that have products with short half-lives, a measurable yield can be produced. Before SLICS can be used for tritium experiments, its performance is being characterized, namely, its ability to measure half-lives on that timescale, that the background rate is not comparable to the number of foreground counts, and for TNSA, that the method of producing and counting isotopes can work at all before a full-scale experiment can be performed. A full-scale TNSA experiment would entail a using a tritium target in the OMEGA 60 chamber at LLE to make a tritium cross section measurement, and while SLICS has been able to detect product nuclei from a TNSA shot at MTW, it has not yet made a cross section measurement, even wi0th deuterons.

1.4. Houghton Experiments

Many experiments have been performed to date to test whether an experiment utilizing ICF or TNSA would be feasible. Testing of the detector system that would eventually be developed into the Short-Lived Isotope Counting System began with experiments in 2016. As previously mentioned, SLICS was designed to measure low energy, light-ion nuclear cross-sections. Figure 4 shows some of the lightest isotopes, along with their half-lives of some elements. Those that are highlighted in green can be created through (d,p), (t,p), (d,γ), and (t,γ) reactions. Notice that they all beta decay with half-lives from about 10 ms to 10 s.

SLICS was designed to measure isotopes that have these characteristics, since a system that can measure all of these products would be useful for measuring the cross-sections of many light ion reactions.

1.4.1. Concept behind SLICS

The system that would eventually become SLICS is based on the concept of a phoswich, or "phosphor sandwich" detector telescope, that is a thin and a thick detector, called dE and E respectively, that are read out by a single photomultiplier. The dE detector measures the rate of energy loss of a charged particle, since as they pass through the dE layer and lose a small amount of energy. The E detector is the thick layer in which the charged particle stops and deposits all its remaining energy.

1.4.2. Summer 2016 Experiment – $^{9}Be(n,\alpha)^{6}He$ with Silicon Detector

The purpose of this experiment was simply to create and detect ^{6}He, which is one of the reactants of interest. The first step towards measuring the radiative capture reaction $^{3}H(t,\gamma)^{6}He$, a reaction shown in Table 1, was to verify that a detector system could be constructed that could detect beta decays from ^{6}He and accurately measure the half-life. This reaction occurs in ICF reactions, but its cross-section has not been measured at any energy both because the cross-section is so small, and no accelerators will produce a tritium beam.

To do this, a silicon detector telescope was constructed using two silicon surface barrier detectors, one which was the dE detector, and one was the E detector, shown in Figure 6. Deuterons from the SUNY Geneseo Pelletron accelerator generated neutrons via the $^{2}H(d,n)^{3}He$ reaction, and these neutrons hit a ^{9}Be target, which produced ^{6}He via the $^{9}Be(n,\alpha)^{6}He$ reaction. Beta decays from the ^{6}He were counted by the silicon detector telescope. This was able to measure the beta particles from ^{6}He decays and found the half-life to be 818 ± 18 ms, which agrees with the previously measured 807 ms. However, a solid-state detector would not survive an ICF implosion, so a new detector was developed that would be durable enough to survive multiple ICF experiments.

1.4.3. Summer 2017 Experiment - $^{9}Be(n,\alpha)^{6}He$ with Phoswich Detector

A similar experiment was performed the next summer to test the efficacy of a new detector which was constructed to be durable enough to withstand the aftermath of an ICF implosion. Plastic scintillator was used, which, when charged particles pass through and deposit energy, gives off light with intensity proportional to the amount of energy deposited. This scintillator was formed into a phoswich, or phosphor sandwich, with a first thin layer with a decay constant of 2 ns, the second thick layer with a decay constant of 285 ns. Once again, the SUNY Geneseo Pelletron accelerator [12] generated neutrons via the $^{2}H(d,n)^{3}He$ reaction, which hit a ^{9}Be slab to produce ^{6}He via the reaction $^{9}Be(n,\alpha)^{6}He$. This half-life was measured to be 789 ± 38 ms, well within the expected uncertainty, meaning that this could be used to measure ^{6}He decays in an ICF or TNSA experiment as well.

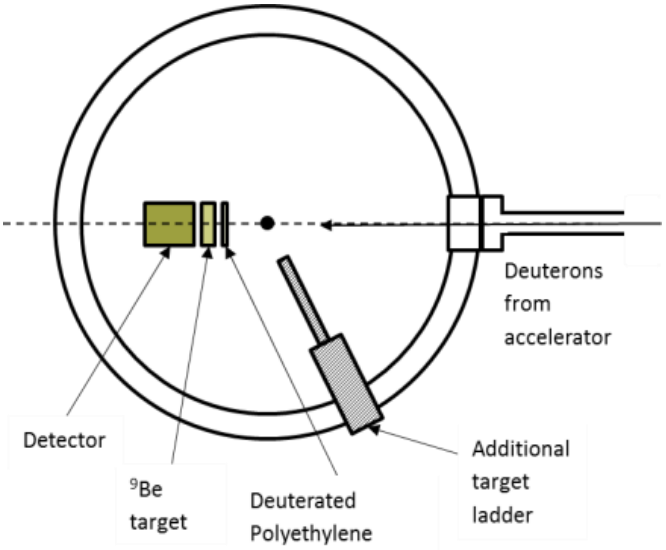

Figure 6. Diagram of summer 2016 experiment. Deuterons from the SUNY Geneseo Pelletron accelerator generated neutrons via the $^{2}H(d,n)^{3}He$ reaction, and these neutrons hit a ^{9}Be target, which produced ^{6}He via the reaction $^{9}Be(n,\alpha)^{6}He$. Beta decays from the ^{6}He were counted by the silicon detector telescope.

1.4.4. Summer 2018 Experiment – $^{40}Ar(d,p)^{41}Ar$

One possible method of measuring low energy light-ion cross-sections that create an inert product like ^{6}He would be to trap the gas which is produced after an ICF implosion as shown in Figure 7. To test the ability of SLICS to trap and detect an inert radioactive gas, ^{41}Ar was produced via the reaction $^{40}Ar(d,p)^{41}Ar$ by accelerating deuterons into an ^{40}Ar gas cell with

the SUNY Geneseo Pelletron accelerator. The isotope ^{41}Ar was chosen because it has similar chemical properties to ^{6}He and beta decays with a similar endpoint energy, but it has a half-life of 109 min rather than the 807 ms of ^{6}He, meaning that this radioactive gas could be produced and transported from SUNY Geneseo to Houghton University. Multiple fast ion gauges were also constructed for this experiment, to measure the pressure at multiple points when the ^{41}Ar gas was released into the test chamber by a fast valve. This is because this trap and detection method would only be successful if the turbopump traps a fixed amount of gas. If gas continues to be trapped after the initial pulse or if gas escapes from the trap, the decay curve would be impossible to measure. The ^{41}Ar was successfully trapped and detected by a silicon surface barrier detector, and the half-life measured to be 109.9 ± 6.6 min, meaning that this method could also be viable for measuring inert gas products of ICF that beta decay.

1.4.5. Summer 2019 Experiment - 4π Detector

To further test the turbopump trap idea, a detector was constructed that was a hollow rectangular prism with wall constructed of phoswich scintillator as shown in Figure 7. After an ICF implosion, the plasma cools and recombines, forming an inert gas. It may be possible to trap this gas and measure the beta particles it would release as it decayed. Since it measured betas in all directions, corresponding to a 4π steradian solid angle, it was called the "4π detector". In the summer of 2019, a similar experiment to that of the previous summer was performed, with the 4π detector instead of a silicon surface barrier detector. Once again, ^{41}Ar was successfully trapped and detected.

1.4.6. Winter 2019 Ride-Along

Another possible idea to trap and detect chemically reactive elements produced by ICF is the getter detector, as shown in Figure 8. With the getter detector, the phoswich detector would be close to the ICF implosion, on the end of a glass light guide which would transmit scintillations from beta particles passing through the phoswich. Chemically reactive isotopes produced by ICF would stick to end of the getter. Two detectors were constructed from the getter and turbopump concepts. To test the background radiation rates for an ICF experiment, the getter detector and 4π detector were both placed outside the OMEGA-60 chamber at LLE during a series of high-yield laser shots using DT filled capsules, which

produced about 10^{14} neutrons. It was found [13] that the maximum count rate for the 4π detector was 350,000 events/s, and 18,000 events/s for the getter. If the capture efficiency of the detector is 1%, the absolute efficiency is close to 100%, and the number of nuclei produced are 10^5-10^7 as predicted in Table 1 with a half-life of 1 s, the estimated product nuclei decay rate is 500,000 events/s within the first half-life. So, the getter detector may have a small enough background rate to use it to make cross-section measurements. Even if it did not, this is not a concern for a TNSA experiment, as there is much less prompt radiation from a TNSA shot. TNSA does not produce the large yield of neutrons that ICF does in each shot, so much less material in the target chamber becomes activated after a TNSA shot.

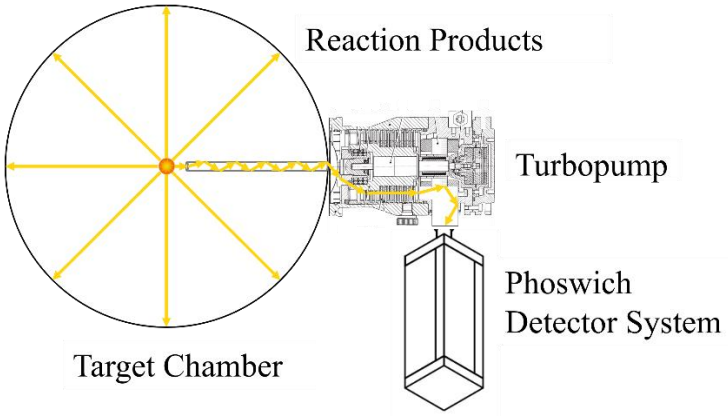

Figure 7. Possible method to trap and detect products of ICF with a turbopump. After an ICF implosion, the plasma cools to recombine and form a neutral gas, and as this gas travels down a collection tube, it would become trapped by the turbopump, and its decays could be detected by a phoswich detector.

1.4.7. Summers 2021 & 2022 – "Exploding Wire" with ^{66}Cu and ^{8}Li

To simulate trapping and detecting the radioactive gas that forms after an ICF implosion, an experiment was performed that used a radioactive isotope that was rapidly evaporated after it was activated. Copper, used in 2021, was electroplated onto a tungsten filament and hit with a deuteron beam from the SUNY Geneseo Pelletron accelerator to produce ^{66}Cu via the reaction ^{65}Cu(d,p)^{66}Cu. A large current pulse then heated up and evaporated the radioactive copper, which then traveled to and stuck on the getter foil at the end of the getter detector. A CAD diagram of this experiment is shown in Figure 9. The ^{66}Cu has a half-life of 5.12 minutes, so the next test was with an isotope that had a half-life on the timescale of other

light ions and was in fact one of the light ions of interest that could be produced with ICF or TNSA, ^{8}Li.

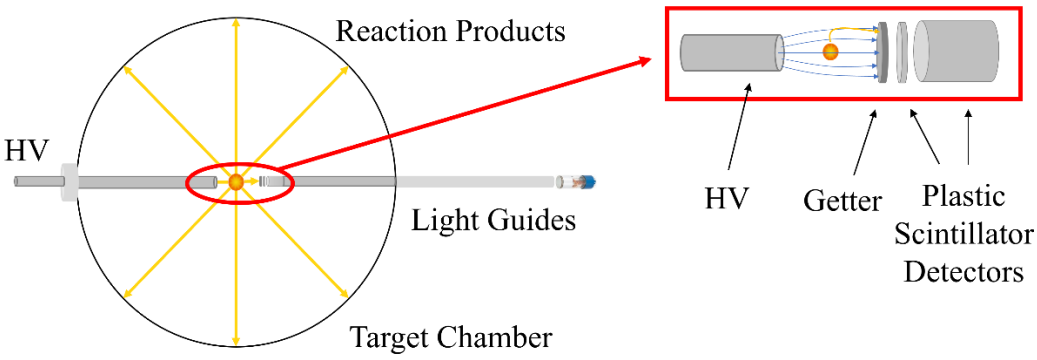

Figure 8. Possible method to trap and detect chemically active products of ICF. One idea is to accelerate product nuclei into the getter using high voltage. The ions would stick to the getter foil on the end of the detector, then beta decay into the phoswich detector at the end of a glass light guide.

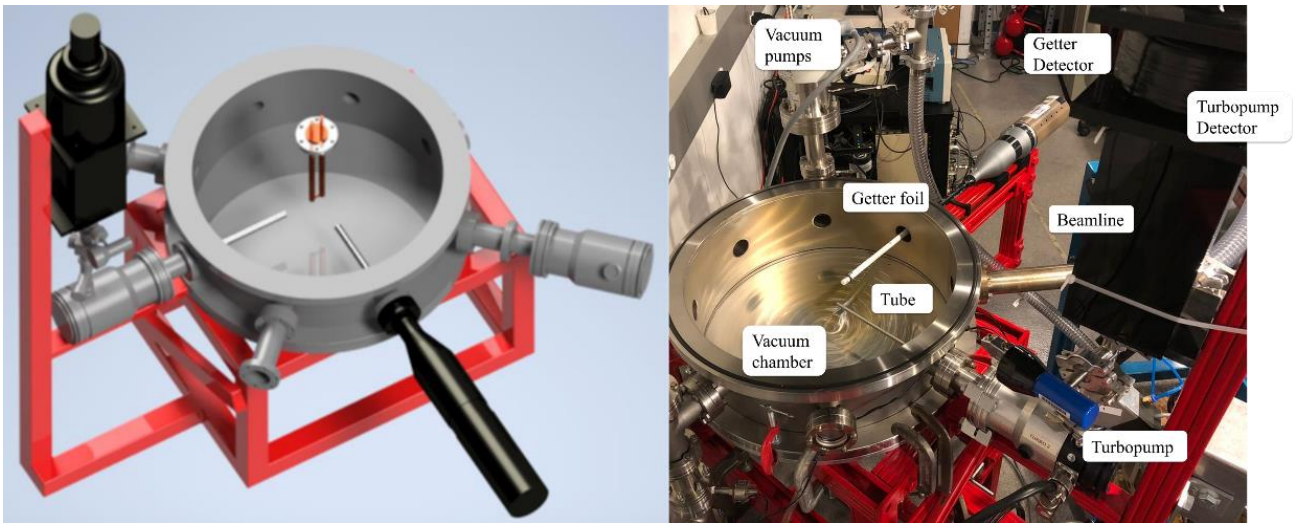

Figure 9. Apparatus of the "exploding wire" experiment. From the orientation of the CAD diagram (left), the deuteron beam entered through the bottom left port and hit the copper-coated tungsten filament in the center of the chamber. A large current pulse passed through the tungsten filament, and evaporated the ^{66}Cu, which stuck to the tip of the getter detector, which faced the tungsten filament.

In order to estimate the efficiency of the detector, a similar experiment to that of the previous summer was performed, with a lithium target instead of a copper target. The half-life of ^{8}Li

is 839 ms, so the success of this experiment showed once again that SLICS has the time resolution necessary to measure the short half-lives of other light-ion nuclear reactions, as ^{8}Li is in fact one of the light ions of interest for the overall goal of this experiment. From this experiment, the absolute capture efficiency of the getter detector in this geometry was measured to be about 7%, which is promising for using ICF to measure cross-sections at low energy. To make the targets, a lithium deposition system was constructed for this experiment, and natural lithium was deposited onto a tungsten target, rather than being electroplated like copper in the previous summer. While this chamber was originally constructed to produce targets for simulating ICF, it was also used for making TNSA nuclear targets.

1.4.8. Summer 2023 TNSA Experiment

In the summer of 2023, an experiment was performed to test the feasibility of TNSA as a technique to measure light ion nuclear cross-sections. As seen in Figure 10, a beam of deuterons was accelerated via TNSA using the MTW laser at LLE towards a natural lithium target. This produced ^{8}Li via the reaction ^{7}Li(d,p)^{8}Li. Beta particles produced by the decaying ^{8}Li were counted via a phoswich detector which was pressed against the nuclear target. This experiment will be described in the remainder of the thesis.

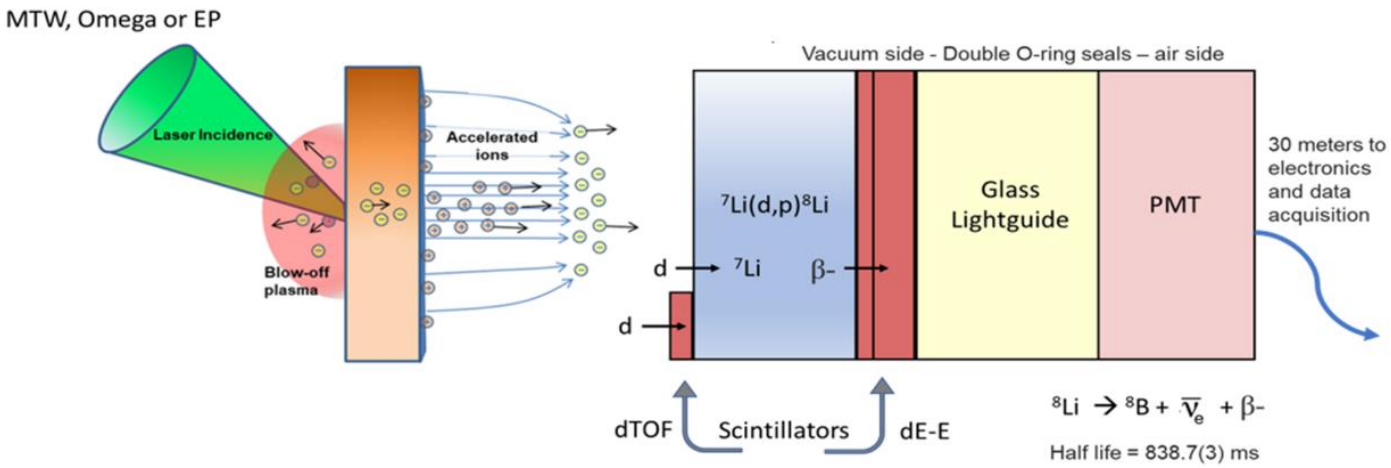

Figure 10. Overview of summer 2023 experiment. A high-power short-pulse laser pulse generated by MTW was incident on a deuterated polyethylene laser target, and positive ions were accelerated off of the opposite side through TNSA. Deuterons produced from TNSA struck a natural lithium nuclear target, and produced ^{8}Li via the reaction ^{7}Li(d,p)^{8}Li. Beta decays from ^{8}Li travelled into the phoswich detector, and light pulses produced by the scintillators traveled through a glass light guide and were recorded by electronics.

Chapter 2

EFFICIENCY AND YIELD CALCULATIONS

This chapter will describe the calculations made to determine the efficiency of the SLICS detector and the initial yield calculations. Efficiency is an important input for the overall goal of this project, to measure nuclear cross-sections, because efficiency relates the number of detected events to the total number of product nuclei that are produced. With the knowledge of the number of reactant nuclei, from either the properties of an ICF capsule or the energy spectrum of deuterons produced by a TNSA laser shot, then the cross-section of the reaction can be calculated.

2.1. GEANT4 Simulation

The simulation code GEometry ANd Tracking (GEANT) was used to estimate the efficiency of the detector. Geant4 [14] is a Monte Carlo simulation tool which was made to simulate the transport of particles and radiation through matter. It can be used to create source and detector geometries composed of various materials, simulate physics interactions and the creation of other particles from reactions, and record data like energy loss of particles in a detector. Figure 11 shows a virtual version of the phoswich detector, using the correct dimensions and materials. Recall that a phoswich detector has two layers: the dE/thin/fast layer and the E/thick/slow layer. Since heavier charged particles like protons and alphas lose energy more rapidly than betas, they usually stop in the dE, depositing all of their energy. The probability of a gamma interacting is roughly proportional to volume, so they are more likely to pass through the thin layer without interacting and deposit energy in the thick layer. So, when the energy deposited in the dE and E are plotted in a 2D histogram, there are regions into which γ, heavy charged particle, and β events fall, as shown in Figure 12. However, betas that travel at oblique angles and take a long path through the dE layer and a short path through the E layer can be stopped in the dE layer and deposit no energy in the E layer, like heavy charged particles. Selecting beta events in the appropriate region on the 2D histogram allows only beta decay events to be considered for analysis.

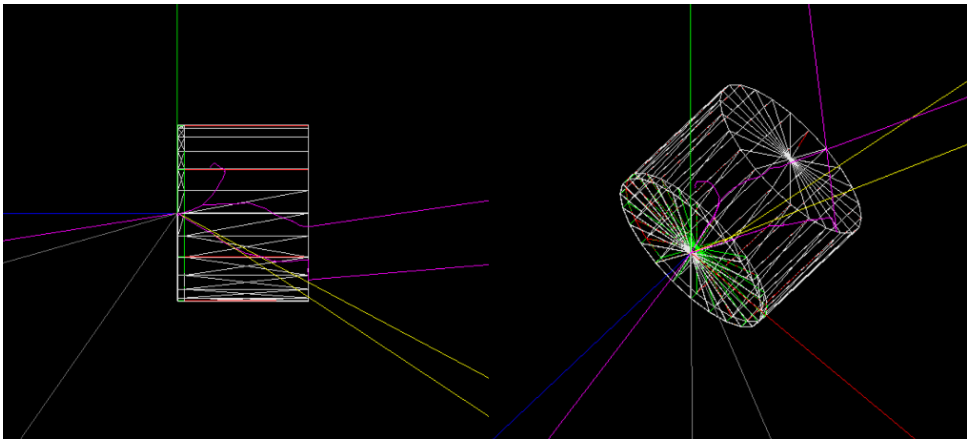

Figure 11. Simulated phoswich detector in Geant4. The detector is shown as a white frame drawing, with the dE layer to the left of the E layer in both images. The magenta lines represent beta particle tracks, yellow lines represent gamma ray tracks. The red, green, and blue lines represent the x, y, and z axes respectively.

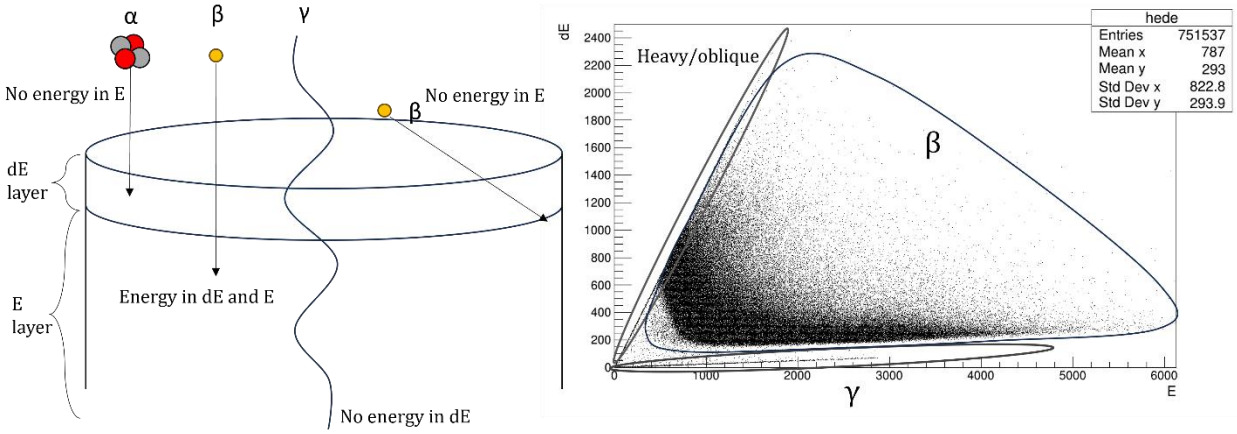

Figure 12. Comparison of different particles hitting the phoswich detector. Heavy charged particles like alphas and protons lose energy more quickly than beta particles, so they deposit most or all of their energy in the dE layer (Left). Beta particles that hit the detector head on travel through and deposit energy in both layers. Gamma rays have a higher probability of interacting with the larger volume, so they mostly interact in the E layer. Beta particles that strike the detector at oblique angles travel through more of the dE layer and less of the E layer, so they deposit energy in a similar manner to heavier particles. Each of these events correspond to a region on a 2D histogram, in which energy deposited in the dE layer is on the vertical axis and energy deposited in the E layer is on the horizontal axis, with units of keV (Right). The 2D histogram was made from a simulation of a ^{8}Li source.

The beta spectrum for ^{8}Li is shown in Figure 13. The energy of the beta particles corresponds to the horizontal E axis. However, above about 4 MeV, beta particles will not stop in the E

detector, and will instead pass through, depositing less than their total energy. This is why the beta energies do not extend to the maximum endpoint energy of about 13 MeV of the ^{8}Li along the E axis in Figure 12.

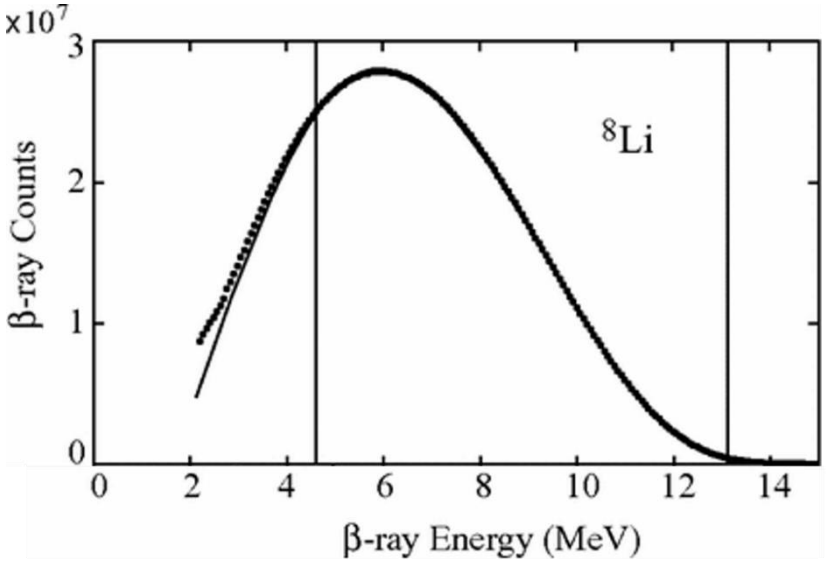

Figure 13. ^{8}Li beta decay spectrum. Notice that in comparison to Figure 12, the density of points on the histogram along the E axis increases with the energy spectrum. However, above about 4 MeV, beta particles will "punch through" and deposit less than their total energy. Taken from Ref. [15]

From the Geant4 simulation, absolute efficiency was estimated by finding the number of events within the selected beta region on the 2D histogram divided by the total number of events

$$f = \frac{n_C}{N} \tag{8}$$

where f is the efficiency, n_C is the number of events within the selected region of the simulation, and $N = 1000000$ is the total number of events that were simulated. The region of the 2D histogram was determined based on simulating the beta decay of ^{207}Bi, which has monoenergetic peaks near 0.5 MeV and 1 MeV as shown in Figure 14. This corresponds to the increased density of points on the 2D histogram in Figure 14 along the E axis. Measurements of the beta decay of ^{207}Bi functioned to calibrate data for this detector, and 2D histogram regions could be selected to only include beta events.

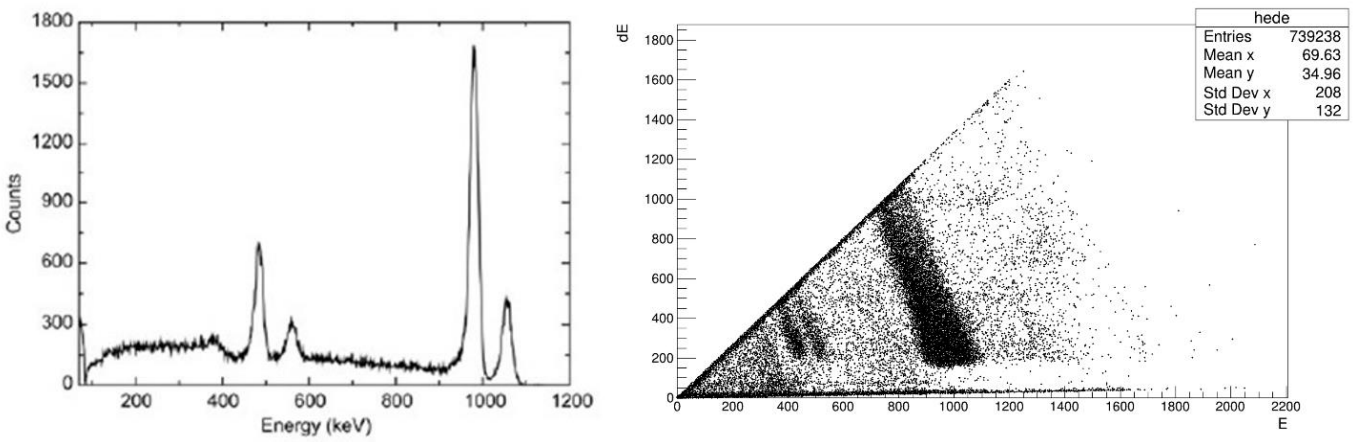

Figure 14. Beta decay of ^{207}Bi. The energy spectrum of the beta decay of ^{207}Bi (left) has two peaks at ~500 keV and two peaks at ~1000 keV. Taken from Ref [29]. This can be seen in the 2D histogram (right) with the total energy of a particles that were detected by a Geant4 phoswich on the horizontal axis, and the rate of energy loss in the vertical axis.

Using this, it was also possible to find the efficiency of the one inch detector when a point source was simulated at the center of the face of the detector. Using equation 8, $f = 46.56\%$.

This is the simplest method of estimating the efficiency of the detector using Geant4. However, the efficiency can be calculated more accurately than just a point source in the center of the detector. Since the detector is cylindrical and symmetric about its axis, moving the source along the radius of the face of the detector is the same as increasing the radius of a ring of sources as shown in Figure 15. For this set of simulations, ^{8}Li point source was simulated 101 times with the location of the source at 0% of the radius for the first measurement, and in each successive measurement the location of the source increased by 1% of the radius, up to 100%.

The area of each ring at radius r with thickness dr is

$$dA = dr\frac{dA}{dr} = 2\pi r\, dr. \tag{9}$$

For some uniform areal density of lithium ρ, the total number of ^{8}Li, dN, in a ring with radius r and thickness dr is

$$dN = \rho(2\pi r\, dr). \tag{10}$$

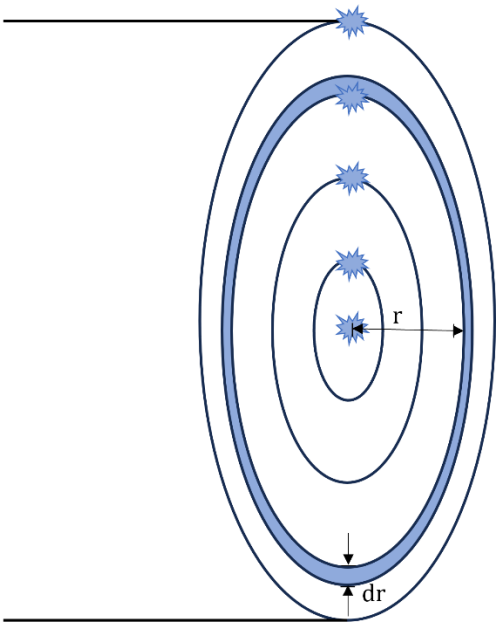

Figure 15. Diagram of source moving along the face of the detector. The shaded symbol represents the placement of a point source, and the ring it lies on is shaded. Since the detector is cylindrically symmetric, the fraction of events detected at each radius will be the same for all points along the ring of that radius. In a ring with radius r and thickness dr, the number of decays in that ring is proportional to the number of nuclei in that ring, which is proportional to its thickness assuming the density of nuclei is constant.

The ratio of detected events dn to the total number of ^{8}Li each ring from radius r to $r + dr$ is the same as the fraction of beta events calculated by Equation (8) from simulation, $f(r)$, so the number of beta particles detected in each ring is

$$dn = f(r)dN = f(r)\rho 2\pi r\, dr. \tag{11}$$

The total number detected in all rings from radius 0 to b is then

$$n(b) = \int_0^b dn = \int_0^b 2\pi\rho f(r) r dr, \tag{12}$$

and the total number of ^{8}Li in all rings from radius 0 to b is

$$N(b) = \int_0^b dN = \int_0^b 2\pi\rho r dr. \tag{13}$$

Thus, the total absolute efficiency $F(b)$ for all rings of radius 0 to b is the total number of detected events divided by the total number of ^{8}Li in all those rings. It is the total number of decays measured divided by the total number of decays, or

$$F(b) = \frac{n}{N} = \frac{2\pi\rho \int_0^b f(r) r\, dr}{2\pi\rho \int_0^b r\, dr} = \frac{2}{b^2} \int_0^b f(r) r dr. \tag{14}$$

Equations (8) and (14) are plotted in Figure 16. The graph for f(r) as a function of distance was determined from the simulation, and F(b) is calculated from these results. For the TNSA experiment, lithium fully covered the target substrate that was pressed against the face of the detector, which had a radius of 1.27 cm. However, the retaining ring put on the face of the detector to hold the target in place covered some of the lithium, so the radius of the spot of lithium exposed to deuterons was 1.14 cm. Thus, two absolute efficiencies of this detector with lithium spots of these radii pressed in front of them are $F(1.27) = 42.27\%$ and $F(1.143) = 45.61\%$.

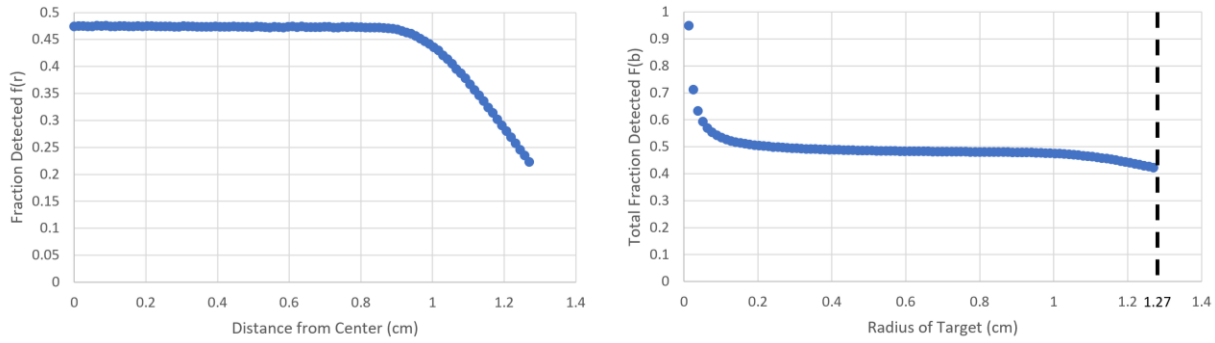

Figure 16. Fraction of betas detected and absolute efficiency of the one inch detector. The fraction of beta particles detected as a function of the radius of the ^{8}Li point source (left) was calculated by the simulation, and the absolute efficiency as a function of target radius for a 1 inch scintillator (right) was calculated from Equation (14).

2.2. Yield Estimate

Ultimately SLICS will be used to measure cross-sections, but for the proof-of-concept experiment performed in the summer of 2023, the yield of ^{8}Li produced by the reaction ^{7}Li(d,p)^{8}Li was calculated based on previous cross-section measurements for this reaction. To measure the cross section, many yield measurements would have been necessary to

deconvolute the cross section. Only a handful of yields were measured, so, for now, only the yield was predicted and compared.

The yield of ^{8}Li, Y, is

$$Y = \int D(E) \cdot N \cdot T \cdot SA \cdot \sigma(E)\, dE, \tag{15}$$

where $D(E)$ is the energy spectrum of the deuterons incident on the lithium target, N is the number density of lithium on the target (^{7}Li/cm^{3}), T is the thickness of the target (cm), SA is the solid angle of the detector (Sr), and $\sigma(E)$ is the cross section of the reaction ^{7}Li(d,p)^{8}Li (cm^{2}). The yield is proportional to the convolution of the energy distribution of incident deuterons with the cross section as a function of energy. The yield detected will depend on the solid angle of the nuclear target, which is 4π times the fraction of the surface area of a sphere with radius equal to the distance from the laser target to the nuclear target. This is proportional to the area of the nuclear target divided by the distance from the laser target,

$$SA = \frac{dA}{r^2}, \tag{16}$$

where dA is the area of lithium which deuterons are incident upon, and r is the distance from the laser target to the lithium. For this experiment, the area of the spot of lithium exposed to the deuteron beam was 4.08×10^{-4} m^{2}, and the two distances from the laser target to the lithium target were 0.375 m and 0.222 m, so the solid angles were 2.90×10^{-3} sr and 8.28×10^{-3} respectively.

The number density N_{Li} of ^{7}Li in the target is

$$N_{Li} = 0.924 \frac{\rho_{Li}}{A_{Li}} N_A, \tag{17}$$

and since natural lithium pellets were used in the deposition process for the nuclear targets. The number density of ^{7}Li in the target is multiplied by a factor of 0.924, since the isotopic composition of natural lithium is 7.6% ^{6}Li, 92.4% ^{7}Li. The number density also depends on the density of natural lithium, $\rho_{Li} = 534$ kg/m^{3} and the relative atomic mass of natural lithium, $A_{Li} = 6.94$ amu, and N_A, Avogadro's number. So, the number density of ^{7}Li was $N_{Li} = 4.28 \times 10^{25}$ cm^{-3}. These calculations were made assuming that there is no oxidation

present on the target, but even if the targets were oxidized, the areal number density of lithium on the target would be the same, since oxidation would cause the target to grow thicker, but the width of the target and the number of ^{7}Li nuclei will stay the same, so the areal number density will stay constant. The thickness of the target is necessary for finding the areal density, which is the number of nuclei per area. This is the product of the number density and the thickness.

Cross-section data for this reaction is taken from the nuclear reaction database Evaluated Nuclear Data File (ENDF), which stores data from multiple evaluated data libraries. The interpreted cross section data for ^{7}Li(d,p)^{8}Li from ENDF and measurements from the joint nuclear database "exchange format" (EXFOR) are plotted in Figure 17. The data from EXFOR disagree, so the interpretation of the data from multiple sources was used for calculations From these values the yield of ^{8}Li produced from each shot can be numerically integrated.

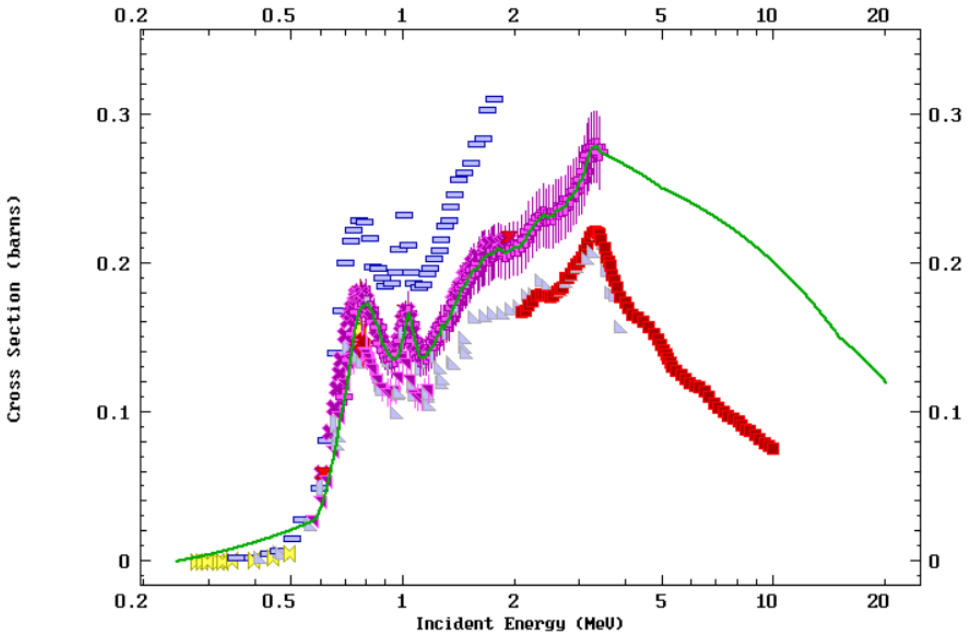

Figure 17. Plot of ^{7}Li(d,p)^{8}Li cross-section measurements as a function of energy. The total cross-section is on the vertical axis, and incident deuteron energy is on the horizontal axis. The points are individual measurements [16 - 24], and the green curve is the evaluated nuclear data file interpolation of these data. Plot generated by EXFOR on NNDC [25].

Chapter 3

EXPERIMENTAL APPARATUS AND PROCEDURE

In this chapter, the experimental apparatus and the procedure will be described. The overall goal for this experiment was to develop a technique to measure nuclear cross-sections using high power short-pulse lasers. As a first step towards this goal, the yield of ^{8}Li nuclei produced by the reaction ^{7}Li(d,p)^{8}Li was measured. The deuteron beam was produced via TNSA using the MTW laser. The yield was determined both experimentally using SLICS and estimated using previously measured values for the cross-section. The thickness of the lithium target was determined by direct measurement with a micrometer and using Rutherford Backscattering. The deuteron energy spectra were measured using time of flight and a Thomson Parabola Spectrometer.

3.1. Experiment Apparatus

Recall from Figure 10 that a high-power, short pulse laser pulse was incident on a deuterated polyethylene target, and protons and deuterons were accelerated via TNSA towards a natural lithium nuclear target. A wedge-shaped scintillator was used as a time-of-flight detector and was used to determine the deuteron and proton energy spectra for each shot. When deuterons struck the nuclear target, the reaction ^{7}Li(d,p)^{8}Li took place. When the ^{8}Li beta decayed, some of the beta particles traveled into the phoswich scintillator which gave off a pulse of light proportional to the energy deposited in the scintillator. This pulse of light traveled through the light guide to the photomultiplier tube, where it was converted to a current pulse which was digitized and recorded. So, each measurement consisted of the production of a pulse of deuterons via TNSA, the reaction of interest ^{7}Li(d,p)^{8}Li taking place, and then a period of 10 s of counting beta decays.

3.1.1. MTW Laser

Each measurement began with the laser pulse. The Multiterawatt laser (MTW) at the Laboratory for Laser Energetics can generate pulses of energy up to 120 J and pulse length of 20 fs to 2.8 ns, but for each shot in this experiment, the energy was ~22 J, and the pulse

length was ~7 ps, meaning the power output was ~3.14 TW. MTW has multiple target areas, but for these measurements the spherical target chamber (STC) was used. Figure 18 shows one of the beam amplifiers, the beamline, and the STC. A top-down view of the STC is shown in Figure 19. The laser pulse traveled down the beamline, was redirected towards the focusing mirror, and then the laser target. Protons and deuterons were accelerated off of the laser target in one burst via TNSA.

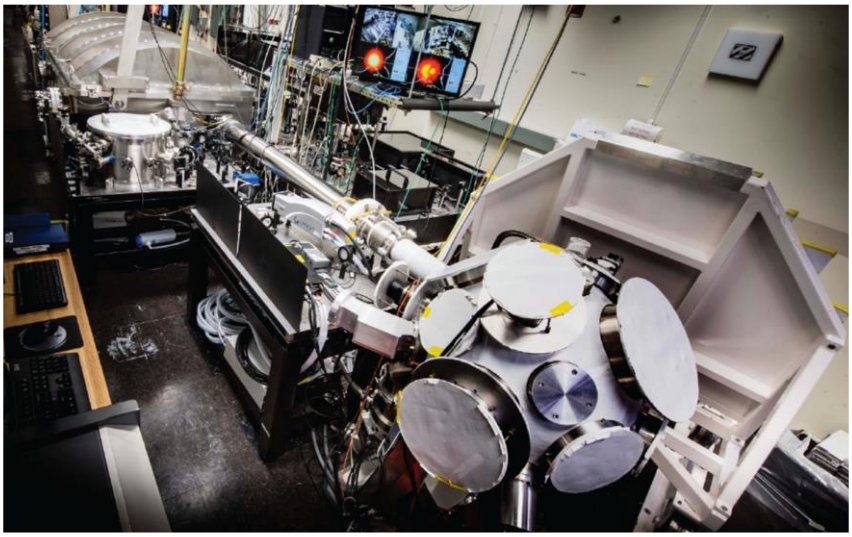

Figure 18. Photograph of MTW. The laser pulse travels through the amplifier at the top left of the photograph, through the beamline, and into the spherical target chamber.

3.1.2. Laser Target

The laser target was a 0.5-mm wide, 25-μm thick deuterated polyethylene square attached to a 5-mm long, 0.08-mm wide stem. In previous studies [7] using the MTW laser, deuterated titanium targets were used due to high electron conductance and a lack of accelerated carbon ions that result from using plastic target. A titanium target would also function well for tritium experiments. In polyethylene the beta decays from tritium would damage the polymer chains, so these targets would damage themselves over time. However, deuterated polyethylene targets are readily commercially available, and can be used to produce deuteron beams with a yield of 10^{11} deuterons, so they were more than adequate for this experiment which was insensitive to carbon ion contamination.

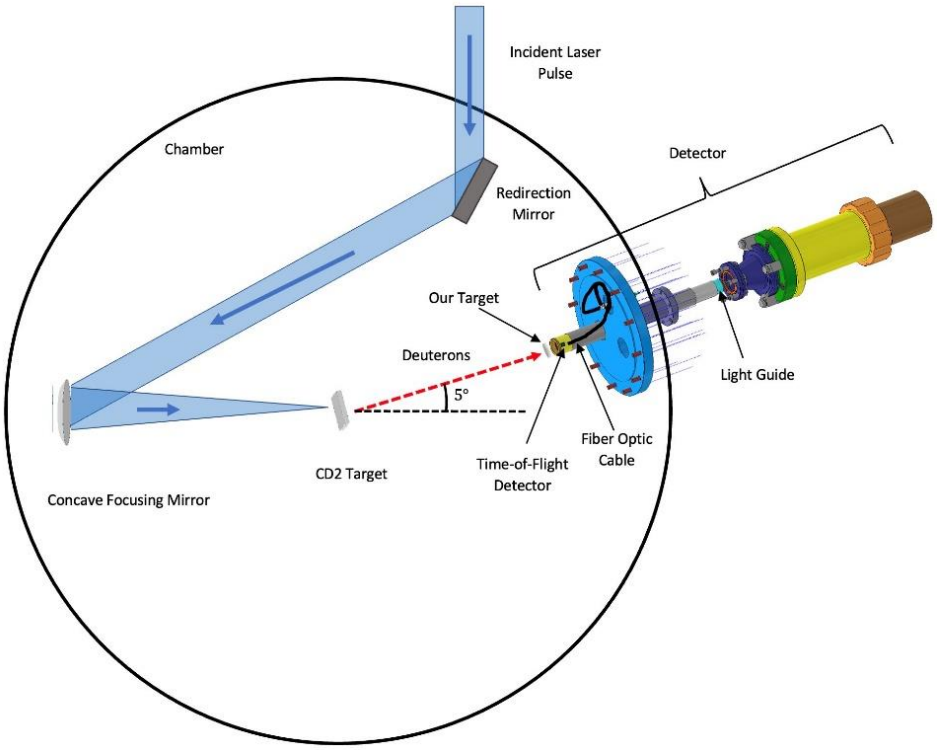

Figure 19. Diagram of the MTW target chamber. The incident laser pulse traveled down the beamline, was redirected towards the focusing mirror, then struck the CD_2 laser target in the center of the chamber. Protons and deuterons were accelerated off the laser target via TNSA. The detector was offset by 5° from the direction of the incident laser beam to prevent the laser pulse from reflecting off the detector and damaging the laser.

3.1.3. Time of Flight Detector

To determine the energy spectrum of protons and deuterons for each shot, a time of flight (TOF) detector was mounted just upstream of the nuclear target. This detector was a $1/16^{th}$ wedge of a 2.54-cm diameter circle of 1-mm thick EJ-200 plastic scintillator. The detector was originally planned to be mounted to the detector as in Figure 20, but light leaked in through the slot where the TOF was mounted. Since the detector measured pulses of light produced by the scintillator, any light leak was unacceptable. For this reason, a separate 3D printed part was created to hold the TOF in front of the detector, and opaque mylar tape was used to cover the light leak.

With such a large number of particles passing through the TOF scintillator, the integrated intensity of light was proportional to the number of particles that passed through as a

function of time, so that the deuteron energy spectrum could be measured from the light intensity as a function of the time-of-flight of the deuterons, and thus their kinetic energy. Figure 21 shows a predicted TOF spectrum from a previously measured MTW deuteron energy spectrum [7]. It was shown that there would be some overlap between slower protons and faster deuterons, since deuterons have twice the mass of protons, so protons will have $\sqrt{2}$ times the speed of deuterons at the same energy, if energy is treated non-relativistically.

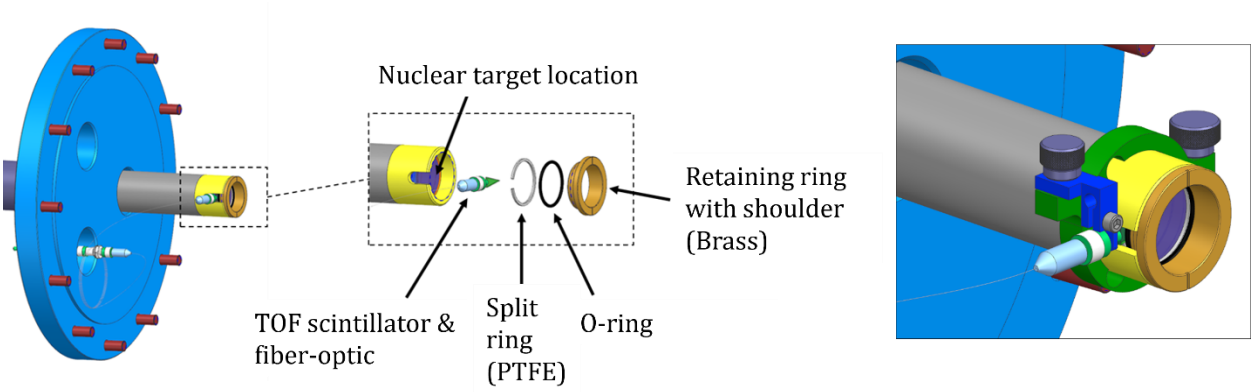

Figure 20. CAD diagram of the phoswich detector. In the original plan for mounting the TOF detector (left), the TOF detector was supported by a slot at the end of the mechanical assembly for the detector and held in place by a retaining ring. This could not be made light tight, so the support used (right) was a 3D printed holder. In the experiment, the holder was on the end of the mechanical support so that the TOF detector was in front of the brass ring, and the slot into which the TOF detector was meant to be inserted was taped over with mylar tape. The fiber optic connected to the scintillator detector exited the target chamber through a separate port.

3.1.4. Nuclear Target

The nuclear target was a 2.54-cm diameter, 25.4-μm thick, 321 type stainless steel substrate with natural lithium deposited on it with a thickness of ~6 to 14 μm and approximately completely covering the stainless steel substrate out to a diameter of ~2.54 cm. The targets were created through physical vapor deposition, and this process took place in a deposition chamber at Houghton. This consisted of a vacuum chamber surrounded by a glove box as shown in Figure 22. The glove box was designed to prevent oxidation of the lithium, because if the lithium target became too oxidized, the additional thickness would cause energy loss of the deuterons, and undesirable isotopes present in the nuclear target. If the target was too

thick, deuterons would lose too much energy in the target, so the actual energy spectrum of the deuterons that activated the target would be significantly different than the measured energy spectrum of the deuterons incident on the target. Since only the incident energy spectrum could be measured using the TOF and the Thomson parabola spectrometer, a thick target would be much more difficult to analyze. Also, oxidation might lead to unwanted nuclear reactions from isotopes other than ^{7}Li on the target, and if the isotopes from these reactions beta decayed, then identification of lithium would be more difficult.

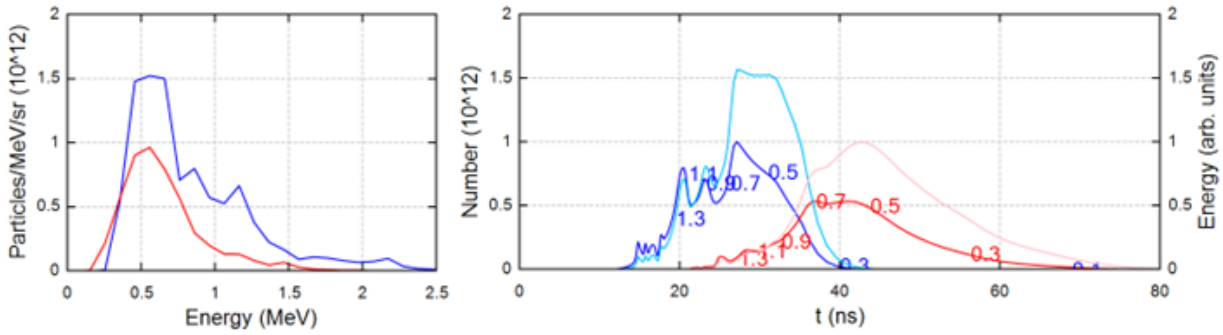

Figure 21. Predicted time of flight for protons and deuterons. (Left) Energy spectrum for TNSA deuterons (red) and protons (blue) from a TiD target using a 7.3 ps long 22.7 J MTW laser pulse [7]. (Right) The calculated resulting deuteron (red) and proton (blue) TOF spectrum 30 cm from the laser target and the energy deposited in the TOF scintillator by deuterons (light red) and protons (light blue) as a function of the TOF. The number axis corresponds to the darker shades, and the energy axis corresponds to the lighter shades. The numbers represent the approximate location of the corresponding deuteron or proton energy in MeV.

The lithium deposition process began by heating up natural lithium until it melted and evaporated. These gaseous lithium atoms traveled upwards and deposited onto the target substrate. The lithium and the tin were held in two separate "boats", tungsten for lithium and molybdenum for tin. The tin was intended to prevent oxidation of the target by depositing a very thin, ~10 nm, thick tin coating onto the target after the lithium was deposited. This would ideally block the lithium from contact with the air while being thin enough to not cause the incident deuterons to lose a significant amount of energy, but unfortunately the targets with tin deposited on them still oxidized. One possible reason for this is that the heating of one boat heated the other boat and the target substrate, which would lead to the mixing of layers. The boat for lithium was heated by passing a current of ~25 A through it,

with much more current necessary to melt tin. A diagram of the two boats used to hold these materials can be seen in Figure 23. Copper electrodes connected the boats to the outside of the chamber, and the positive and negative leads of the power supply were switched to heat each boat. Diodes were placed so that current would only flow through one boat at a time during the deposition process. The lithium and targets were handled in a glove box which was filled with argon, an inert gas, which would not oxidize the lithium.

Figure 22. Photograph of the lithium deposition chamber. The glove box was filled with argon to prevent oxidation of the lithium in air. Two pairs of gloves were accessible from the outside of the glove box for handling at multiple heights. The two leads of the power supply were connected to the copper electrodes on the face of the deposition chamber.

The thicknesses of the nuclear targets were determined in two methods: a direct measurement using a Mitutoyo IP54 micrometer and Rutherford Backscattering spectrometry (RBS). The micrometer was a precise caliper, which was unable to distinguish between layers of oxygen and lithium. With RBS, protons or alpha particles were accelerated using the SUNY Geneseo Tandem Pelletron Accelerator, and the energies of incident particles

which were scattered backwards were used to determine the thickness and elemental composition of the target. One of the energy spectra is shown in Figure 24.

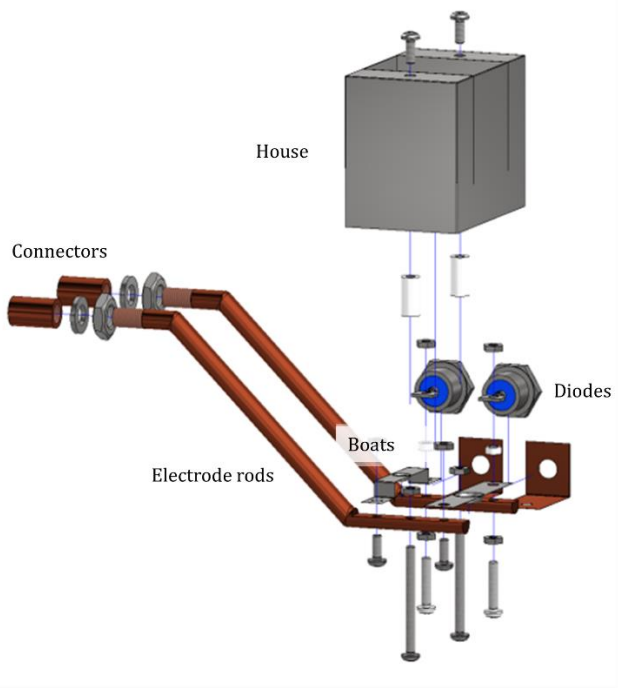

Figure 23. CAD drawing of lithium deposition boats. One boat held natural lithium, the other held tin, which was deposited after the lithium to prevent oxidation in air. Diodes were placed at the end of each boat so that current would only flow through one boat at a time. A house was placed over both boats to prevent lithium and tin from coating the chamber.

3.1.5. Phoswich Detector

After ^{8}Li was created on the nuclear target, the ^{8}Li beta decayed, and some of the beta particles traveled into the phoswich detector. Recall that the phoswich detector was composed of two layers as shown in Figure 25. The dE layer was a 25.4-mm diameter, 1-mm thick EJ-200 plastic scintillator with a decay time of 2.1 ns and the E layer was a 25.4-mm diameter, 18-mm thick EJ-240 plastic scintillator with a decay time of 285 ns. As charged particles passed through the phoswich, the dE and E layers each gave off flashes of light that overlapped in time. This pulse traveled down the 25.4-mm diameter, 308 mm long Schott F2 glass light guide, passed through a 69.9-mm diameter, 6.4-mm thick Schott F2 glass window, and was then recorded as a voltage pulse via a Burle 8575 photomultiplier tube. Figure 26 shows an example of a pulse from the photomultiplier tube displayed on an oscilloscope.

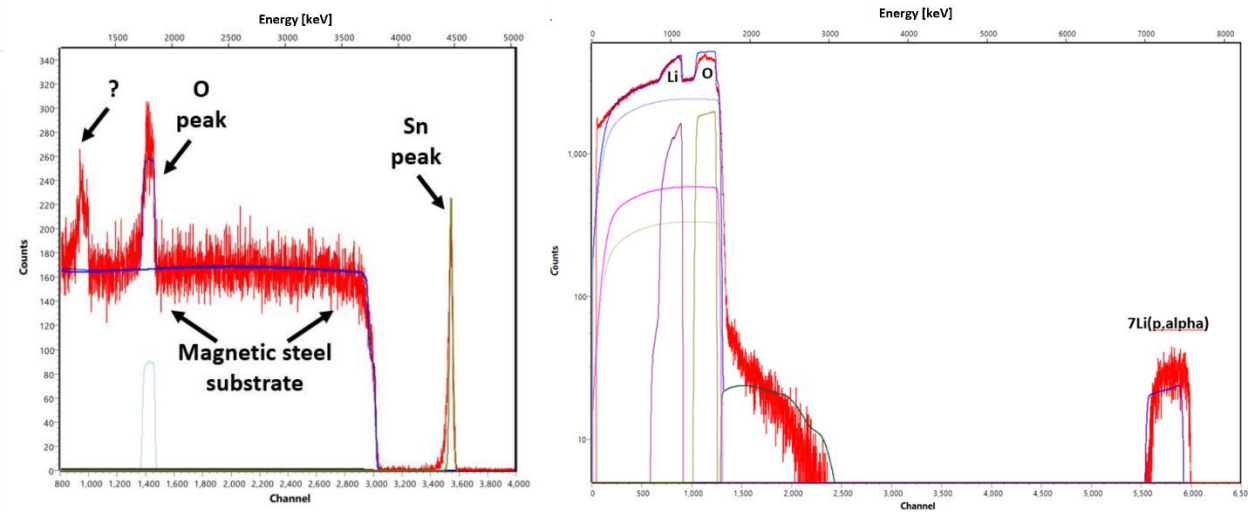

Figure 24. RBS Energy Spectra. The number of counts in each channel, which is proportional to energy, is plotted. A 5.1 MeV alpha particle beam (left) was incident on the target, and the predicted features of the tin coating and steel substrate are visible, as well as a peak which indicates oxidation, which was also expected. A 2.0 MeV proton beam (right) was incident on the target which cause the nuclear reaction ^{7}Li(p,α) to occur.

The mechanical assembly which supported the phoswich, light guide, window, and photomultiplier tube is shown in Figure 27. The large flange connected to the MTW target chamber. The 2.75" CF nipple could be exchanged for multiple lengths to change the distance between the laser target and the detector.

Before the detector could be placed in the MTW target chamber, it had to be shown that the detector would not outgas any materials that could coat or impair the performance of optics in the MTW target chamber or upstream in the laser system. In the months prior to the experiment, a two-layer test phoswich was epoxied together, but when tested by heating to 90°C in a vacuum, cracks appeared. Pieces of acrylic were epoxied together and put in vacuum at Houghton, and no cracks appeared. Later tests at Houghton revealed that a critical step in the process of epoxying the plastic together had been skipped for the test, which is placing the EJ-500 epoxy and resin mixture in vacuum to remove bubbles before applying it to the surface. Two test pieces of acrylic were epoxied together with epoxy that was not put in vacuum first, and when this assembly was put in vacuum, cracks and bubbles were clearly observed, as is shown in Figure 28.

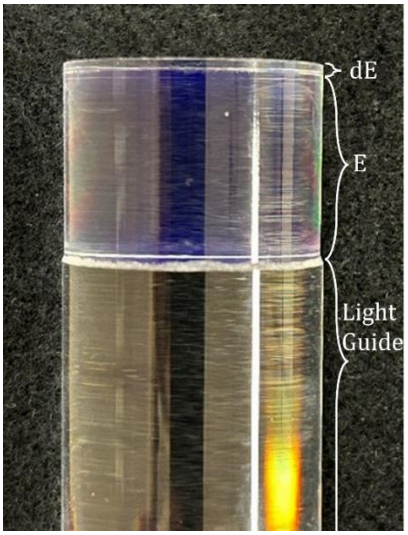

Figure 25. Photograph of phoswich detector. The 25.4 mm diameter, 1 mm thick dE scintillator was epoxied to 25.4 mm diameter, 18 mm thick E scintillator, which was epoxied to 25.4 mm by 308 mm glass light guide.

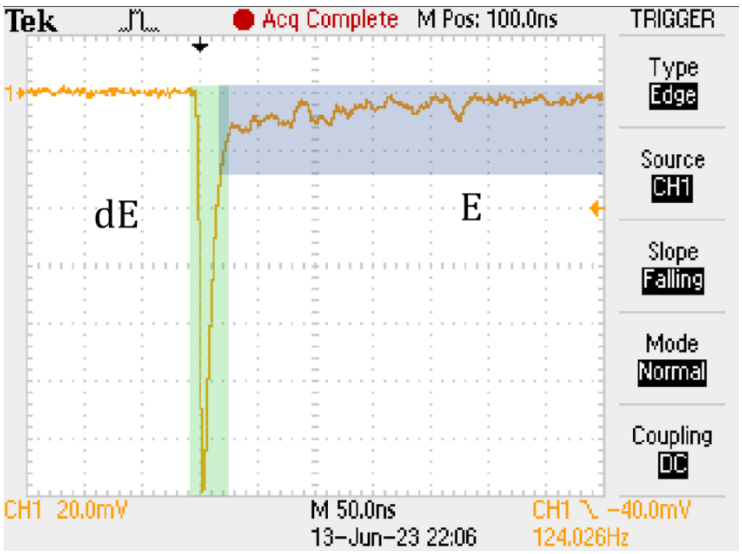

Figure 26. Oscilloscope trace of pulse from the phoswich detector. The green highlighted dE region is the part of the pulse that was produced from charged particles passing through the thin/fast scintillator, and the blue highlighted E region is the part of the pulse that was produced from charged particles passing though the thick/slow scintillator. These pulses are separated in time. The integral under these pulses is proportional to the energy deposited in each layer. The integral of the dE region of the pulse is proportional to how quickly the particle loses energy, and the integral of the E section of the pulse is roughly proportional to the total energy of the particle.

3.1.6. Electronics

To remotely control the timing of the experiment and to record the sampled pulses the phoswich detector, a computer-controlled circuit was constructed, as shown in Figure 29. To protect the electronics from the EMP produced by the laser shot, the original design had the photomultiplier tube electrically isolated from the rest of the electronics via an isolation relay circuit, but the Sensata-Cynergy3 DAT70515 relays picked up so much noise in the MTW lab that the data would not be viable, so the isolation circuit was not used for this experiment. It seems that electrical signals produced by other electronics in the room, possibly sparking that produced radio waves, was picked up in the wire between the contacts of the relays, which is much less shielded against electrical pickup than the BNC cables the signal traveled through outside of the relays.

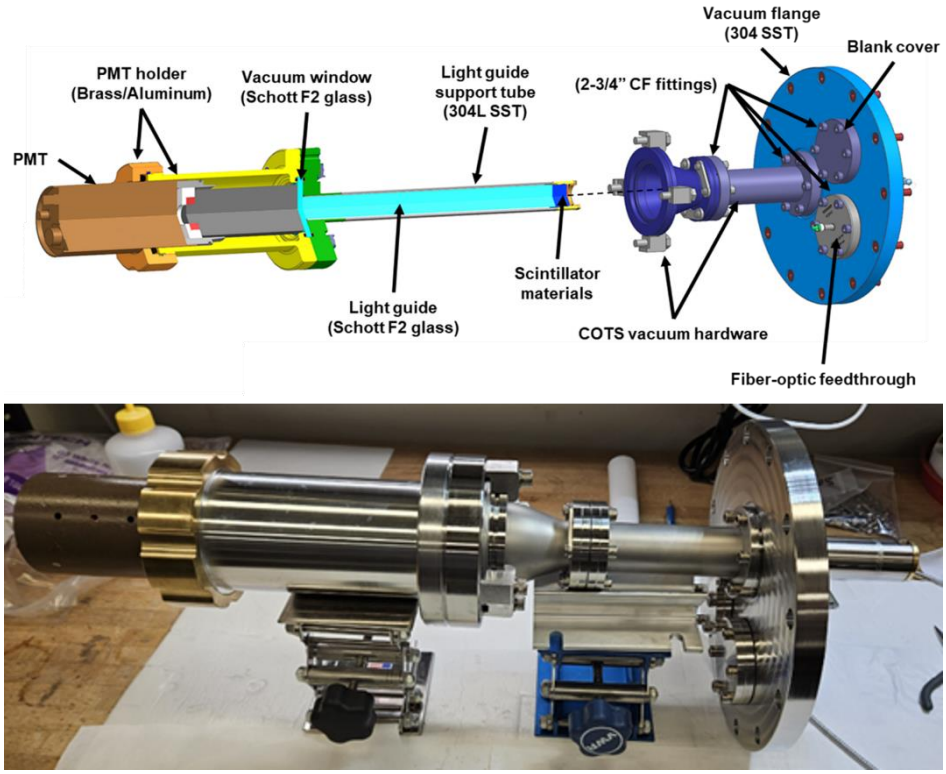

Figure 27. CAD drawing and photograph of detector support. The detector assembly which was used (bottom) was built to the specifications of the CAD diagram (top). The vacuum seal was maintained by O-rings on either side of a Schott F2 glass window which was optically coupled to the light guide and PMT with EJ-550 Silicone Grease. The detector was kept light tight by the support system, with opaque mylar tape on the end of the assembly to cover the slot for the TOF.

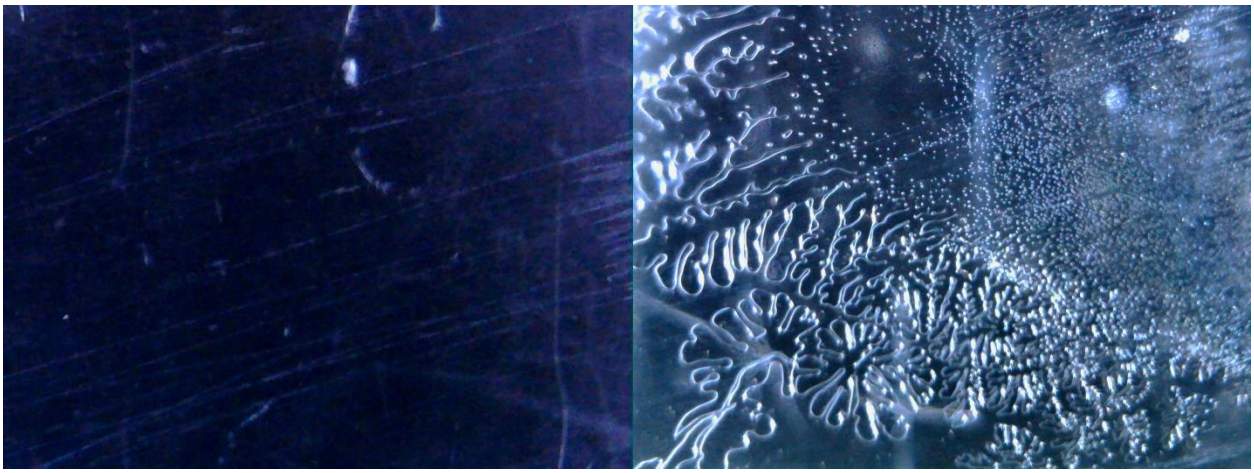

Figure 28. Photograph of epoxy on test acrylic. The uncracked epoxy (left) only had marks from scratches on the surface. The cracked epoxy (right) was made by not putting the epoxy resin mixture in vacuum to remove bubbles before application, and then heating the epoxied acrylic in vacuum after the epoxy hardened.

The MTW control system produced a 5 V, 400 ns TTL pulse for each laser shot, and this functioned as the trigger signal for the data acquisition system. It was sent to the detector electronics system concurrent with the laser shot, where it was converted to a 3.3 V, 5 μs CMOS pulse via 416A ORTEC Gate and Delay Generator, so that this pulse was compatible with the GPIO inputs of the Raspberry Pi 4 which controlled the timing of the experiment. The Raspberry Pi delayed for 2 ms after it received this pulse, then closed the relays to connect the HV to the PMT and the signal to the digitizer, as well as the grounds via the MOSFET circuit shown in Figure 30. Once the relays were closed, the flashes of light produced by the phoswich were converted to voltage pulses via a Burle 7585 photomultiplier tube and digitized by a CAEN N6730SB digitizer, which sampled pulses every 2 ns for a 400 ns interval around the pulse. The pulse heights also were recorded by a Skutek Instrumentation DDC 10 digitizer, which was included in this experiment for comparison with the CAEN digitizer. For every pulse the CAEN digitizer received, it triggered the DDC 10 so that the same pulses were digitized by both digitizers.

The control code for the Raspberry Pi is included in Appendix A. After receiving the trigger pulse from the MTW control system, the Raspberry Pi sent the signal to close the relays. The

relays took at most 2 ms to stop bouncing, so the Raspberry Pi delayed 2 ms until starting the CAEN and DDC 10 digitizers to avoid noisy signals while the relays were bouncing.

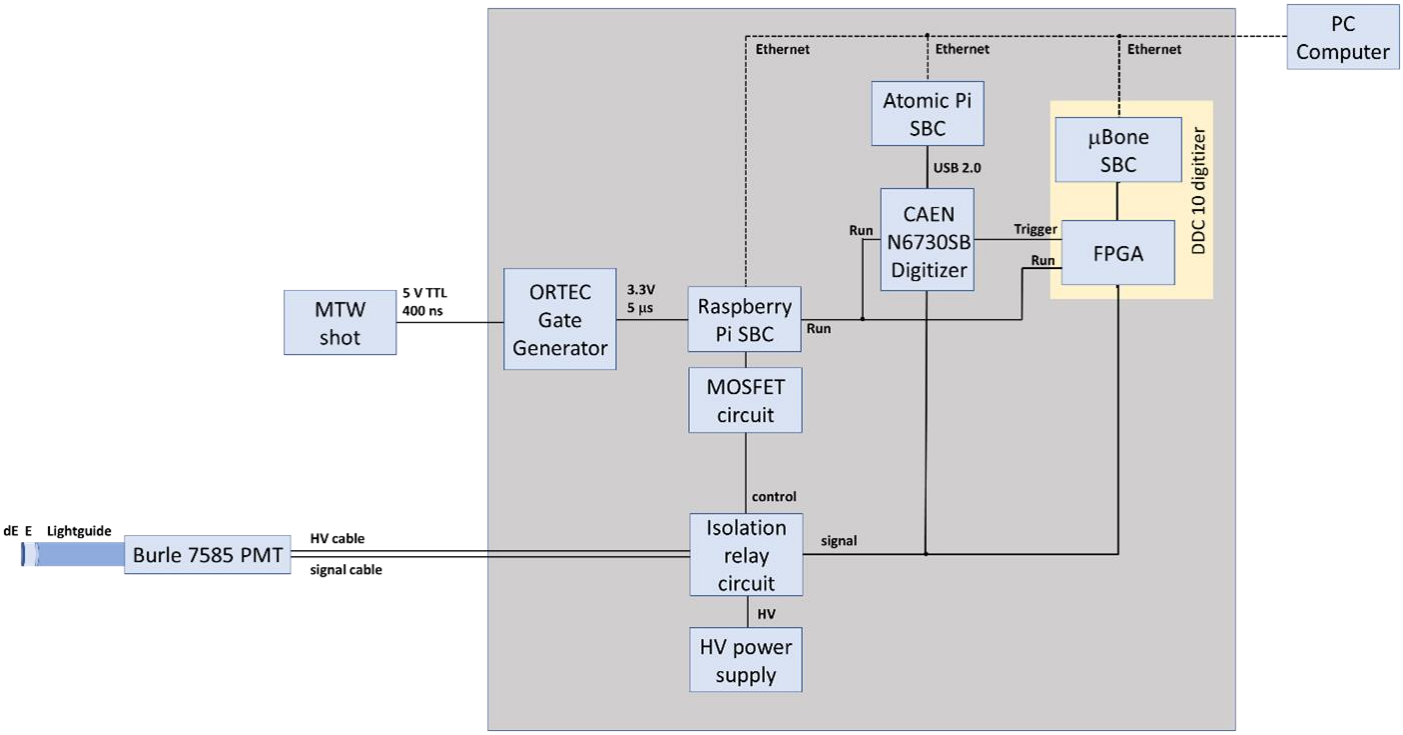

Figure 29. Block diagram of the electronics. A TTL pulse from the MTW system was converted to a CMOS pulse via the ORTEC Gate Generator. This triggered the Raspberry Pi to close the relay circuit after 2 ms. Once this happened, the photomultiplier tube powered on, and light pulses produced by the phoswich detector passed through the light guide, were converted to a current pulse by the photomultiplier tube and were digitized by CAEN digitizer and DDC10 digitizer. These digitized pulses were then stored in a PC.

3.1.7. Thomson Parabola Spectrometer

The energy spectrum of protons and deuterons produced by each TNSA shot was also measured with a Thomson parabola spectrometer. This device uses parallel electric and magnetic fields to separate ions based on charge and energy. The path of a particle through the Thomson Parabola is shown in Figure 31. Viewed from the same orientation as the image plate in Figure 32, the electric field and magnetic field are pointed to the right, and so ions deflect to the right based on their charge to mass ratio from the electric field, and ions deflect upwards based on their kinetic energy, mass, and charge

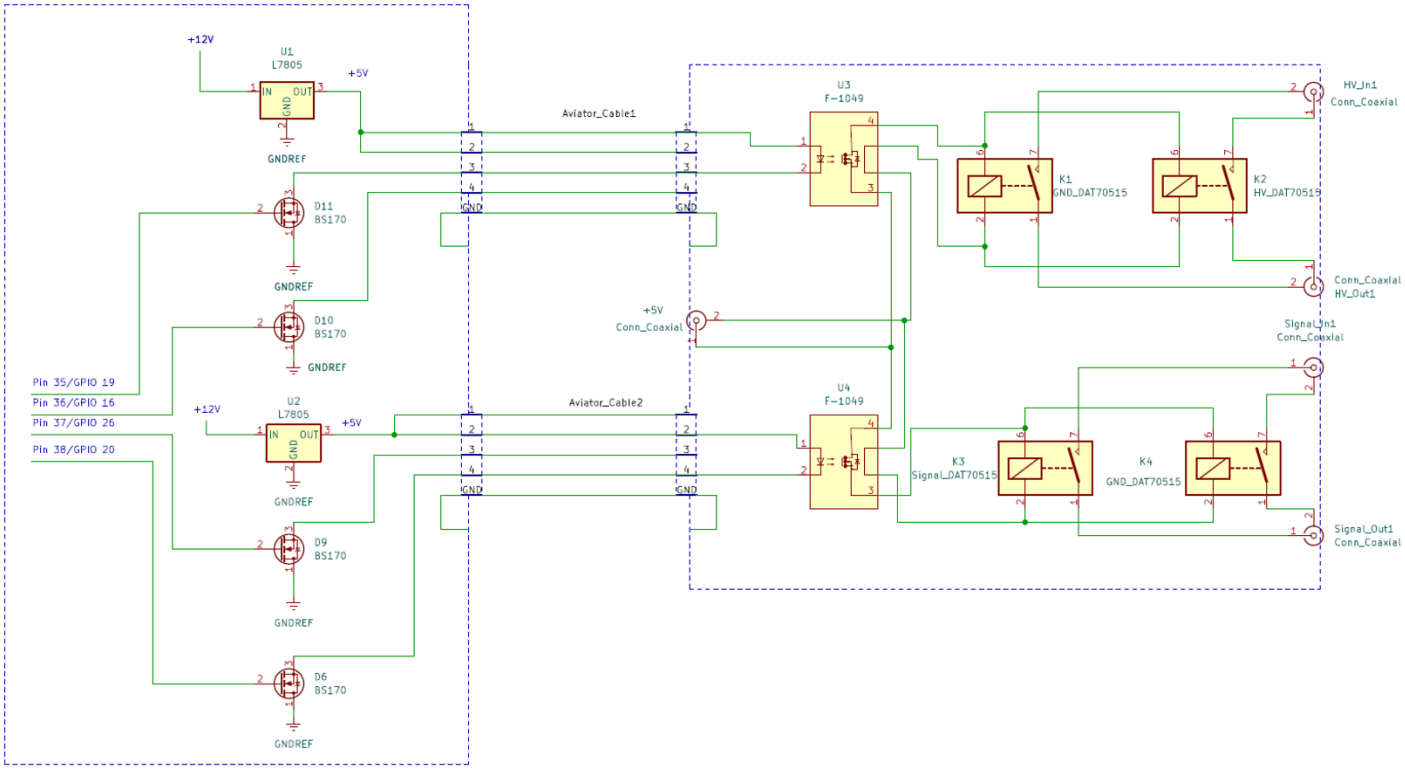

Figure 30. MOSFET circuit schematic. The GPIO pins on the Raspberry Pi controlled MOSFETs which powered solid state relays. These solid-state relays powered high speed isolation relays through which the HV and signal for the PMT passed. Multiple relays were required to reduce noise in the PMT signal.

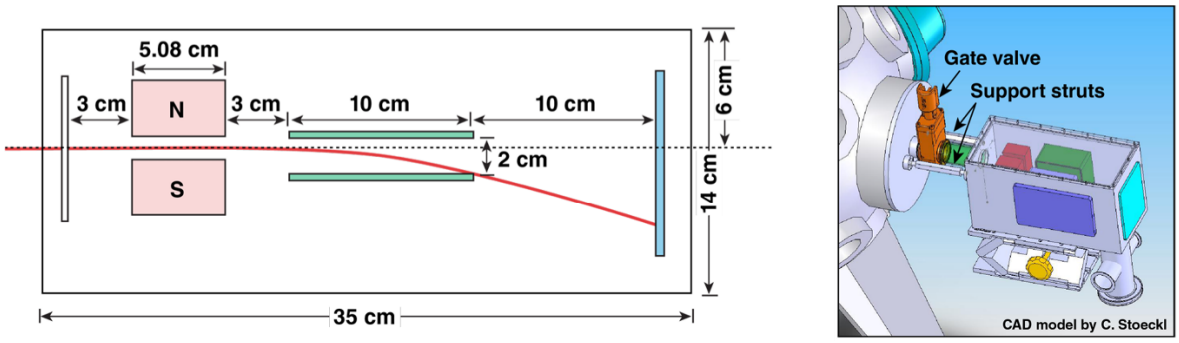

Figure 31. Thomson Parabola diagrams. The block diagram (left) shows a top-down view of a particle's path through the Thomson Parabola. Each particle first passed through a pinhole which collimated the beam of particles, then a permanent magnet, which deflected ions out of the page based on velocity and charge-to-mass ratio. They then passed through an electric field, which deflected ions down based on their charge-to-mass ratio. Each particle then struck an image plate, where its position was recorded for later analysis. In both the block diagram and the CAD drawing (right) of the Thomson Parabola, red signifies the magnets, green signifies the electric plates, and light blue signifies the image plate. Figure taken from Ref [26].

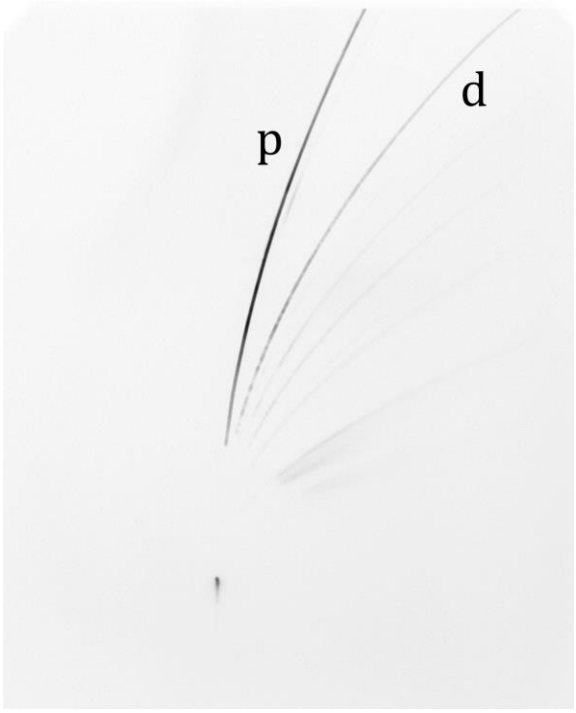

Figure 32. Thomson Parabola Spectrometer image plate. Parallel electric and magnetic fields in the spectrometer separated ions by mass and energy. Protons, deuterons, and multiple charge states of carbon were blown off the deuterated polyethylene target via TNSA, and traveled through a pinhole before they were deflected. Protons were deflected from center the least, followed by deuterons.

Chapter 4

ANALYSIS AND RESULTS

The previous chapter described the experimental apparatus and procedure of the experiment. This chapter will discuss the data collected and the analysis of those data. The data obtained from SLICS was first used to determine the half-life and thus the identity of the isotope detected, and then the ^{8}Li yield produced by the reaction ^{7}Li(d,p)^{8}Li. This was done by selecting beta events from 2D energy histograms, then plotting the total number of beta events as a function of time and extracting the yield from the growth curve fit. The data from the TOF detector and Thomson Parabola Spectrometer were used to determine the energy spectra of the deuterons and protons produced by TNSA. From the deuteron energy spectrum, the number density of lithium, the solid angle of the detector, and previous cross section measurements for ^{7}Li(d,p)^{8}Li, the yield was also predicted and compared with the experimental measurements.

4.1. Half-life Results

From the growth curve of each measurement, both the yield and the half-life can be extracted. If the half-life measured was that of ^{8}Li, the yield would indeed be for the reaction ^{7}Li(d,p)^{8}Li. Otherwise, if the half-life was not that of ^{8}Li, then some other isotope was activated in a much greater quantity than lithium, and the data from these measurements are not useful for calculating the ^{7}Li(d,p)^{8}Li yield or cross-section.

To determine the isotopes that were activated, the half-life was determined from the detected decay events. Each time the isotope that was activated beta decayed it released a beta particle, some of which traveled into the phoswich detector which gave off a pulse of light with intensity proportional to the energy deposited in each layer. This pulse of light was converted to a current pulse by the photomultiplier tube and was then sampled every 2 ns for 400 ns. Each waveform which was recorded by the CAEN digitizer also included a timestamp. So, by plotting the number of beta events over time, a decay curve was created.

Integrating the decay curve gave a growth curve. The growth curve was fit with an exponential function to determine the half-life and yield could be determined.

First, the beta events were selected. A typical 2D histogram of dE-E pulses is shown in Figure 33. The red quadrilateral selects beta events and excludes the dense region of noise in the lower left corner. When the timestamps of these events were plotted, the number of events over time exponentially decayed, and the half-life of the beta source could be determined. The red quadrilateral which selected beta events was chosen both from a Bi-207 measurement, which was used due to the 0.5 MeV and 1 MeV electrons Bi-207 emits, which are easily distinguishable from heavy charged particles and gamma rays. The quadrilateral was also chosen to avoid the dense portion of measured events in the lower left of each 2D histogram. When examining individual pulses from this region, they are like the digitized pulse in Figure 34. These pulses had multiple peaks with no tails, rather than the expected beta pulses which had one peak with a long tail, so these pulses were noise and thus disregarded.

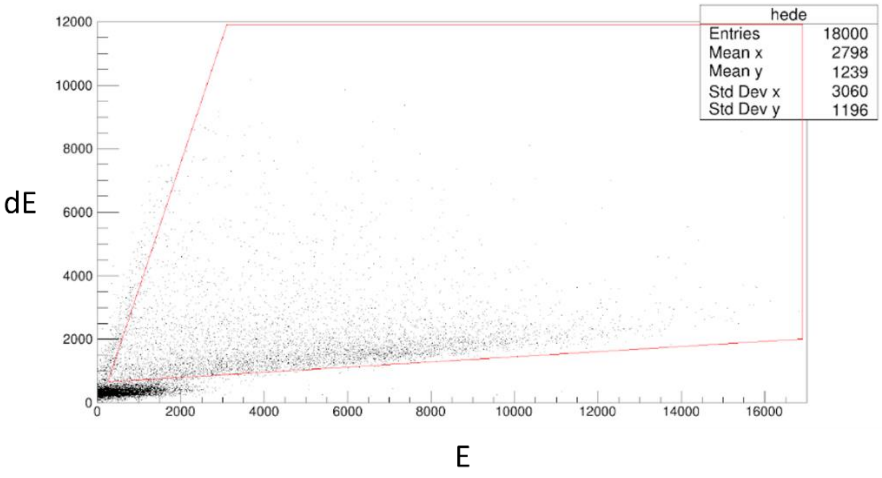

Figure 33. 2D histogram data from MTW shot 15978. The energy deposited in the thin dE layer, which is proportional to the rate of energy loss of a particle, is plotted on the vertical axis, and the energy deposited in the E layer, which is proportional to the total energy of a particle, is plotted on the horizontal axis. The density of dots represents the number of beta events at that energy. The red border around a portion of the data selects only beta decays.

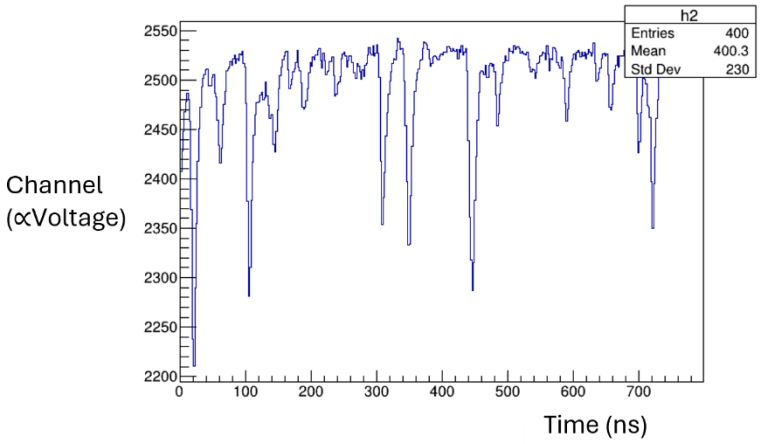

Figure 34. Digitized noise pulse. This is an example of a pulse from the lower left region of Figure 33. Rather than having one peak with a long tail like the form of a dE-E beta event, they had multiple peaks with no tails, so they were noise and were disregarded.

Recall from Chapter 1 that the number of some decaying radioactive isotope N at some time t is described by the decay equation

$$N(t) = N_0 e^{-\lambda t} + B \tag{18}$$

where N_0 is the number of nuclei at $t = 0$, and λ is the decay constant of the decaying isotope. Background can be accounted for by assuming that it is constant, B. Integrating this equation from 0 to some time t yields the growth curve,

$$N(t) = N_0\left(1 - e^{-\lambda t}\right) + Bt. \tag{19}$$

The decay constant can be determined by fitting Equation (19) to the integrated number of counts over time. Once the decay constant is determined from the fit, the half-life is then known by $t_{1/2} = \ln 2/\lambda$. After the half-life was calculated and it was confirmed that ^{8}Li, then the yield that was simultaneously determined by fitting Equation (19) was known to be that of the reaction ^{7}Li(d,p)^{8}Li.

Figure 35 is an example of a measured decay and growth curve. The decay plot shows the number of counts in 1 ms time bins, and the growth curve is the integral of these counts. The growth curve is more advantageous for determining N_0 because after a few half-lives, the total number of counts is $\sim N_0$. So, the fit for the growth curve is generally better for

determining N_0, whereas the decay plot will be $\sim B$ after a few half-lives and is better for determining B.

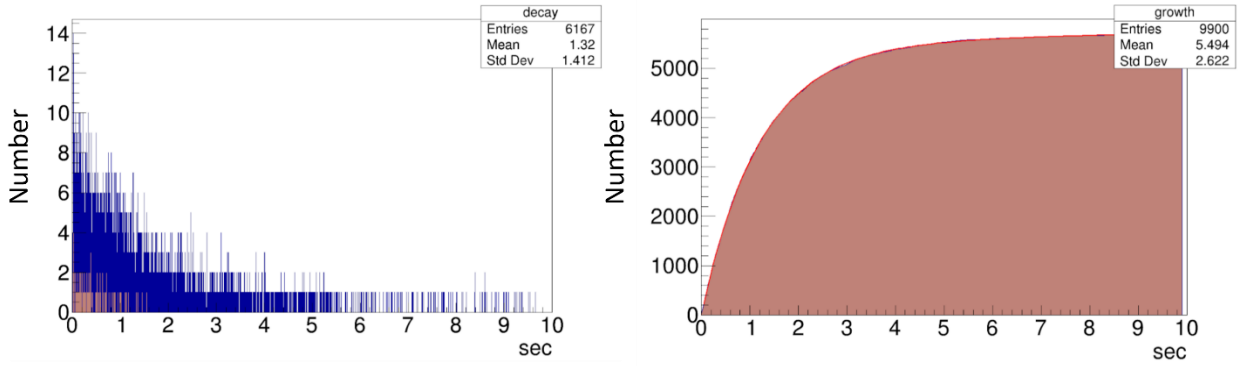

Figure 35. Decay and growth curve for MTW shot 15978. The decay curve (left) shows the number of counts in each 1 ms wide time bin. The growth curve (right) plots integrated number of counts over time. Equation (19) was fit to the growth curve graph, from which the yield was determined. The red growth curve fit line is overlayed on the

These plots were fit using the MINUIT [27] package of ROOT [28]. ROOT is a software framework used for data analysis which was written for scientists at CERN, and MINUIT is a package which fits data by minimizing the chi-squared value. To obtain a more accurate value for N_0, the total number of decays, the decay constant was fixed to that of ^{8}Li, $\lambda = 0.82645\ \mathrm{s}^{-1}$.

Table 2. Growth curve fit values. Fit values and error were determined by MINUIT. Error in N_0 is much less than N_0

MTW Shot Number	N_0	Error in N_0	B	Error in B
15975	3559	1.65	25.63	0.274
15976	2064	0.83	4.70	0.205
15978	5509	2.03	20.64	0.331
15984	2000	1.23	7.96	0.203
15988	3144	1.69	44.84	0.304
15990	2486	1.41	33.74	0.237
15991	4677	1.90	29.09	0.316

The number of ^{8}Li nuclei could be determined from the growth equation. Immediately after the target was activated, the counts were too high for the digitizer to keep up, and so some time bins were empty while the digitizer was reading out. So, the time histogram fit usually began about 200 ms after the trigger from the MTW control system was received. The maximum value determined from the growth curve, N_0, is the number of ^{8}Li decays that were detected starting at 200 ms. The number of ^{8}Li when the TTL signal from the MTW laser system is received, which is $t = 0$, can be determined by the decay equation

$$N_{t=0} = N_0 e^{-\lambda(200\text{ ms})} \tag{20}$$

rearranged to solve for N_0. This will not be the total number however, since this is reduced by the absolute efficiency of the detector, as not every beta particle traveled into the detector. Dividing by the efficiency gives the experimentally measured value for the yield of ^{8}Li. Table 3 shows this value calculated for multiple runs. The difference between values is most likely due to differences in target thickness.

Table 3. Experimental yield results. The laser parameters were determined by the MTW system. Each lithium target had an areal density which was measured by both a micrometer and RBS. The distance from the laser target to the detector was changed to vary the solid angle. The yield was determined from the growth curve.

MTW Shot Number	Laser Energy [J]	Laser Pulse [ps]	Nuclear Target Number	Nuclear Target Thickness (micrometer) [μm]	Nuclear Target Areal Density (micrometer) [10^{19} atoms / cm^2]	Nuclear Target Areal Density (RBS) [10^{19} atoms / cm^2]	Distance to target [mm]	Yield
15975	18.6	13.6	15	6.0	2.78	1.96	375	9331
15976	18.9	13.3	15	6.0	2.78	1.96	375	5412
15978	19.5	11.6	20	9.0	4.17	1.26	375	13297
15984	13.5	12.1	17	13.7	6.35	4.10	375	5244
15988	13.5	11.8	12	3.7	1.71	0.94	222	15965
15990	13.1	11.6	20	9.0	4.17	1.26	222	7078
15991	13.3	11.2	20	9.0	4.17	1.26	222	12778

4.2. Time-of-Flight Results

The time-of-flight scintillator was mounted so that protons and deuterons incident on the lithium target were also incident on the TOF. This was used to determine the energy spectra

of the protons and deuterons for each measurement. Measurements were made with the laser pulse incident on a CH target, which produced protons via TNSA, and measurements with a CD target, which produced both protons and deuterons via TNSA. The TOF detector produced light with intensity proportional to the amount of energy deposited in it over time, and this light was converted into a current via a photomultiplier tube. From the amount of energy deposited over time and the distance of the laser target to the TOF, the speed and thus energy of the protons and deuterons was calculated. The current as a function of time for laser targets is graphed in Figure 36. From the difference in the proton and deuteron spectrum and the proton spectrum, the deuteron spectrum was determined. From the deuteron spectrum in Figure 37, the relative number of deuterons was determined. However, this was not calibrated, so the number of deuterons at each energy for the yield calculation cannot be determined from the TOF data.

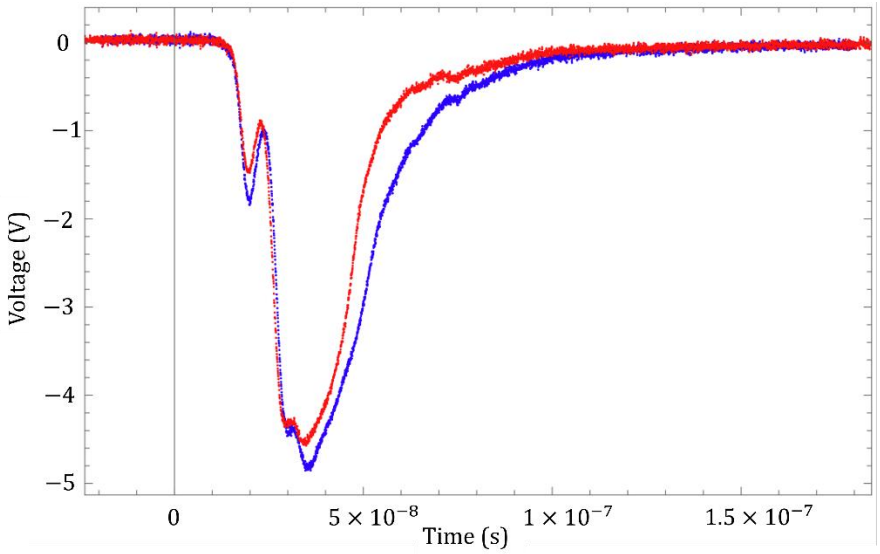

Figure 36. CD (blue) and CH (red) spectra from TOF detector. As protons and deuterons passed through the TOF scintillator, it gave off a continuous pulse of light with intensity proportional to the energy deposited in it. This light was converted to a current pulse. The voltage over time into 50 Ω, which is proportional to the energy deposited over time, is plotted. With a CH target (red), protons were accelerated from the target. With a CD target (blue), protons and deuterons were both accelerated. The deuteron energy spectrum is then the difference in these two voltages.

4.3. Thomson Parabola Results

To obtain calibrated measurements for the deuteron energy spectrum with separated proton and deuteron spectra, measurements were taken with a Thomson Parabola Spectrometer. Similar laser parameters were used with CH_2 and CD laser targets, and ions that accelerated via TNSA that passed through a pinhole were deflected based on charge to mass ratio and kinetic energy. After deflection, the particles struck a BAS-SR image plate, and each plate was scanned with a photo stimulated luminescence machine which recorded the x- and y-coordinates of each pixel on the scan, along with each pixel's relative intensity. From the deflection in each direction, the energy spectra of the deuterons could be plotted, as shown in Figure 38. The deuteron spectra for CH targets gives an idea of the uncertainty in this measurement since deuterons and protons overlap in the low energy region.

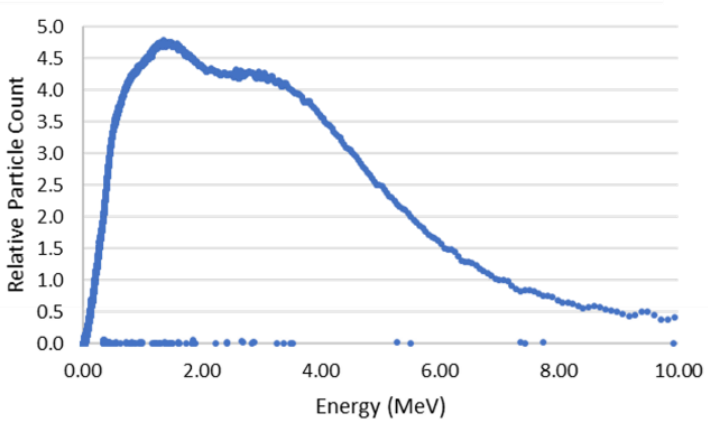

Figure 37. Relative energy spectrum for deuterons. From the time after the laser pulse and the distance from the laser target to the nuclear target, the velocity and thus the kinetic energy of the deuterons was calculated. Light intensity was not calibrated, so no yield calculation could be made from them.

The Thomson Parabola was mounted at 0°, but the detector was offset by 5° during ^{8}Li measurements, and this introduced more uncertainty into the energy spectrum results. When the target was offset by 5°, the laser pulse was incident on the target in the same direction it was during ^{8}Li measurements, so the beam spot on the target was the same size, but ions were accelerated normal to the target, so less ions hit the Thomson Parabola than in ^{8}Li measurements. However, when the target was offset by 0°, the target was facing the

Thomson Parabola in the same orientation it was facing the lithium target during ^{8}Li measurements, but the beam spot on the target was smaller, so the laser pulse was more intense, so ions were accelerated at a lower energy, in fewer number than ^{8}Li measurements. It was believed that beam spot size on the target had a greater effect on the deuteron energy spectrum, so the measurement in which the laser was offset by 5° was used for yield calculations.

4.4. Yield Results

The yield was determined from Equation (15) after the energy spectra of the deuterons was determined from the Thomson Parabola data. This comparison is shown in Figure 39. For most laser shots, the experimental value for the yield of ^{8}Li produced by the reaction ^{7}Li(d,p)^{8}Li was within about a factor of two of the predicted yield which was calculated using the thickness of the lithium target which was determined by RBS. The yield prediction which used micrometer data was greater than the experimental value in most cases because the micrometer measured the total thickness of the target, which includes oxidation. This is not ideal but considering that this was a proof-of-concept experiment, a factor of two is promising for the future of this experiment.

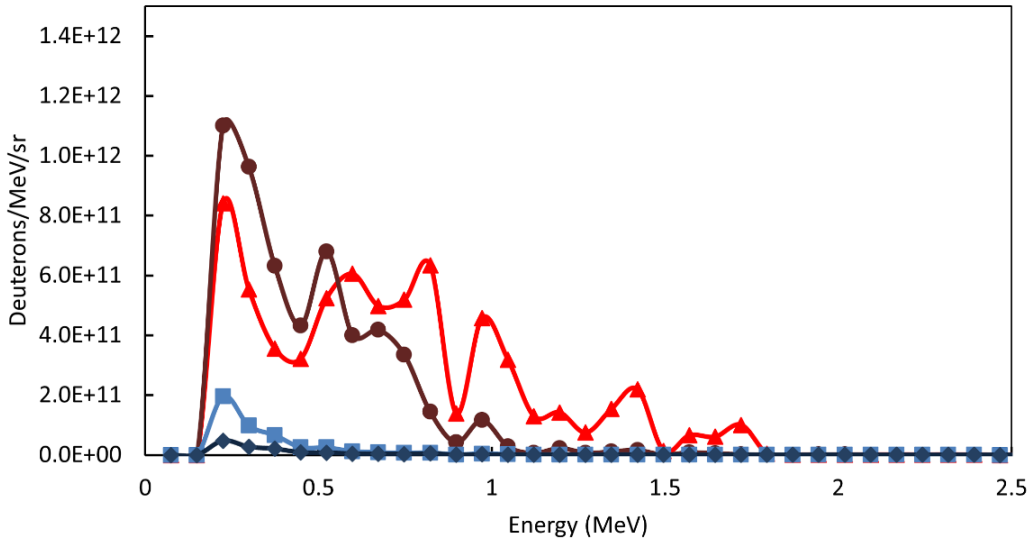

Figure 38. Graph of the deuteron spectra as a function of energy. From the deuteron spectra from deuterated polyethylene targets (brown/circle, red/triangle), the number of deuterons at each energy can be determined. The deuteron spectra for polyethylene targets (light blue/square, dark blue/rotated square) are shown for comparison. For two of the measurements (brown, light blue), the target was offset from the direction of the laser pulse by 5°, as it was in ^{8}Li measurements and Figure 19. For the other measurements (red, dark blue), the target was offset by 0°. The number of deuterons is divided by the solid angle of the pinhole.

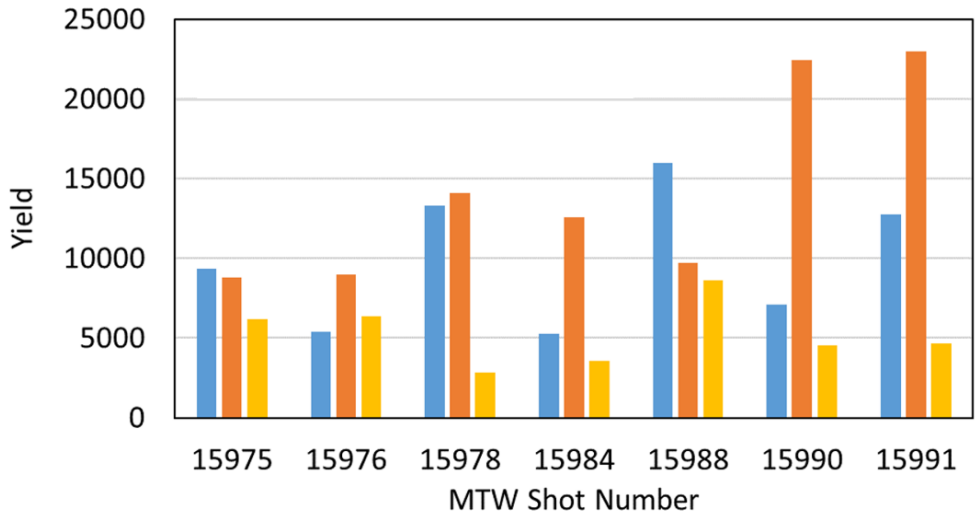

Figure 39. Yield comparison for prediction and experiment. The blue bars are measured yields of ^{8}Li from the reaction ^{7}Li(d,p)^{8}Li that were calculated from the growth curve fit of experimental measurements. The orange and yellow bars are predictions of the yield from Equation (15), where the thickness for was determined using a micrometer (orange) and RBS (yellow). The energy spectrum of the deuterons used for this calculation was the Thomson Parabola measurement in which the deuterated polyethylene target was offset by 5°, since it was believed that the angle of the laser relative to the face of the target had a greater impact on the energy spectra than the orientation of the laser target to the lithium target.

Chapter 5

CONCLUSIONS AND FUTURE PLANS

5.1. Summer 2023 Experiment Conclusions

The overall goal of this experiment is to develop techniques using high power, short pulse lasers, to measure light ion nuclear cross-sections that have not been measured before. This could possibly be done using advances in high power, short pulse laser technology, such as ICF and TNSA, which produce a large yield of nuclei in a short time. These methods could also be used to study triton induced reactions, which would not be possible in traditional accelerator experiments. The Short-Lived Isotope Counts System (SLICS) has been developed through multiple experiments beginning in 2016. The most recent step towards this goal was a proof of concept experiment in which TNSA was used to accelerate deuterons towards a lithium target and produced ^{8}Li through the reaction ^{7}Li(d,p)^{8}Li. A phoswich detector was placed directly behind the lithium target, and detected beta particles that were produced from ^{8}Li beta decaying. The number of beta events was plotted over time, and fit with a growth curve, and from this growth curve the number of ^{8}Li detected was determined, from which the yield was calculated. The yield was also predicted using the energy spectrum of incident deuterons, the thickness of the lithium target, the number density of lithium on the target, the solid angle of the detector, and previous cross section measurements for the reaction ^{7}Li(d,p)^{8}Li. Experiment and prediction agreed within a factor of two for most measurements. This is promising, given that this was a proof of concept experiment.

The results of this experiment are a promising step and show that not only TNSA can be used to produce nuclear reactions, but SLICS can be used to identify the isotope produced by the reaction and measure the yield within a factor of 2.

5.2. Future Plans

There are multiple directions the experiment could take in the future. In order to measure the cross section of a reaction, many more yield measurements would need to be made to allow the cross section and energy spectrum to be deconvoluted. Only a few yields were

measured in this experiment, using previous cross section measurements, but if greater care was taken to reduce uncertainties in the thicknesses of lithium targets and the deuteron energy spectra, then the cross section for ^{7}Li(d,p)^{8}Li could be determined with a similar experiment in MTW.

Further experiments could be performed with tritium as well, considering that the potential for tritium induced reactions is one of the main motivations these high-power short pulse laser experiments. These experiments would take place in the OMEGA 60 target chamber at LLE, which is built to handle tritium. A SLICS detector would be inserted into the chamber using a ten-inch manipulator (TIM) diagnostic inserter, which is standard for LLE. One possibility is the TNSA experiment shown in Figure 40. The OMEGA EP laser would be used for this experiment, since it can generate shorter laser pulses which could be used for TNSA. A laser target would contain tritium, and tritons would be accelerated via TNSA off the laser target towards a lithium target.

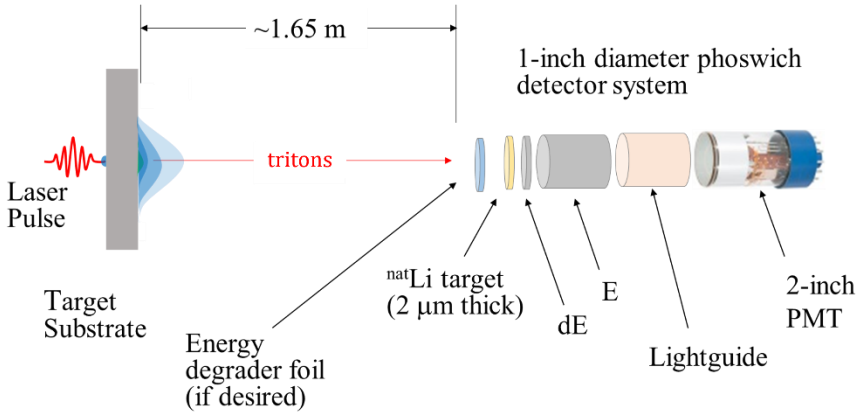

Figure 40. Tritium TNSA Experiment. In this experiment, the target would be doped with tritium, so that tritons would be accelerated via TNSA. These tritons would strike a natural lithium target, and the reactions ^{6}Li(t,p)^{8}Li would take place. Then, some of the beta particles produced by ^{8}Li beta decaying would then be detected by SLICS.

Inertial Confinement Fusion is another option for measuring low energy, light ion nuclear cross-sections, as is shown in Figure 8. The ICF target capsule would be filled with deuterium or tritium, and doped with another isotope of interest, like ^{6}Li, ^{7}Li, or ^{9}Be. The isotope would be selected based on the predicted yield, given in Table 1. A SLICS detector would be placed

in the OMEGA 60 target chamber, and chemically reactive isotopes produced in the ICF implosion would stick to the getter detector. The detector high voltage and signal would be kept electrically isolated from the rest of the electronics until a few ms after the ICF implosion, to protect the electronics from the EMP which would result from the ICF implosion. Once the relays would be closed, then counting could begin, in an environment with much less noise than immediately after the reaction.

Appendix A

Below is the code for the Raspberry Pi 4 that controlled the timing of the experiment. Originally, this code was intended to open and close the isolation relays, but for the actual measurements it waited to trigger the CAEN and DDC10, dependent on the trigger pulse sent by the MTW control system.

```
#include <stdlib.h>
#include <stdio.h>
#include <pigpio.h>

// to compile:  gcc SLICS.c -o SLICS -l pigpio

int main(int argc, char *argv[])
{

float duration;
int secs, microsecs;

// Read in the commend line arguments
if(argc!=2) {
   printf("Usage: SLICS <duration>\n");
   printf("   duration = length of time to enable digitizers (s)\n");
   exit(0);
    }

duration = atof(argv[1]);
printf("Enabling digitizers for %f seconds.\n",duration);

secs = duration;
microsecs = (int)((duration - secs)*1000000);
printf("  %d secs  %d microsecs\n",secs, microsecs);

// Initialize the pigpio library
if (gpioInitialise() < 0)
   {
   fprintf(stderr, "pigpio initialisation failed\n");
   return 1;
   }

/* Set GPIO modes */
gpioSetMode(2, PI_OUTPUT);    // enable CAEN digitizer when high
gpioSetMode(3, PI_OUTPUT);    // enable DDC10 digitizer when low (External
veto,DDC10 input 3)
gpioSetMode(12, PI_OUTPUT);   // Reset timestamp (DDC10 input 3)
gpioSetMode(19, PI_OUTPUT);   // HV relay
gpioSetMode(16, PI_OUTPUT);   // HV ground relay
gpioSetMode(26, PI_OUTPUT);   // signal relay
gpioSetMode(20, PI_OUTPUT);   // signal ground relay
```

```
gpioSetMode(13, PI_INPUT);    // laser trigger input

// turn everything off
gpioWrite(2,0);
gpioWrite(3,1);  // enable when low
gpioWrite(12,0);
gpioWrite(16,0);
gpioWrite(19,0);
gpioWrite(20,0);
gpioWrite(26,0);


// wait for pulse from laser control
while(gpioRead(13) == 0){   }

// Delay turning on HV?
// gpioSleep(PI_TIME_RELATIVE, 0,5000);  // secs + microsecs

// turn on relays
gpioWrite(16,1);
gpioWrite(19,1);
gpioWrite(26,1);
gpioWrite(20,1);

// start digitizers
// Delay to wait for relays to stop bouncing
gpioSleep(PI_TIME_RELATIVE, 0 , 2000);
gpioWrite(2,1);     // enable CAEN
gpioWrite(12,1);    // reset DDC10 timestamp (assuming leading edge)
gpioWrite(3,0);     // enable DDC10
gpioWrite(12,0);    // end pulse for reset timestamp

// Wait while data are collected
printf("Run Started\n");
gpioSleep(PI_TIME_RELATIVE, secs,microsecs);  // seconds+ microseconds

// End of experiment -- turn everything off, disable digitizer
gpioWrite(2,0); // stop CAEN digitizer
gpioWrite(3,1); // stop Femtodaq
gpioWrite(16,0);
gpioWrite(19,0);
gpioWrite(20,0);
gpioWrite(26,0);

gpioTerminate();

return 0;
}
```

R e f e r e n c e s

[1] R. Woods, J.L. McKibben, and R.L. Henkel, Nucl. Instrum. Methods **122**, 81-97 (1974).
[2] United States Government Accountability Office, Report to the Committee on Armed Services, U.S. Senate, Report GAO-15-272, (2015).
[3] E. Loomis et al., Los Alamos National Laboratory Report LA-UR-05-0775, (2005).
[4] L. H. Gresh, *Inertial Confinement Fusion: An Introduction* (University of Rochester, Rochester, 2009).
[5] A.J. Koning, S. Hilaire and M.C Duijvestijn, "TALYS-1.0", Proceedings of the International Conference on Nuclear Data for Science and Technology, April 22-27, 2007, Nice, France, editors. O. Bersillon, F. Gunsin, E. Bauge, R. Jacqmin, and S. Leray, EDP Sciences, 211 (2008).
[6] S.N. Abramovich, B. Ya. Guzhovskij, V.A. Zherebtsov, and A.G. Zvenigorodskij, International Nuclear Data Committee Report INDC(CCP)-326/L+F, (1991).
[7] A. Schwemmlein, Ph. D. Thesis, (University of Rochester, 2021).
[8] A. Einstein, Phys. Z. **18**, 121 (1917).
[9] T.H. Maiman, Phys. Rev. Lett. **4**, 11 (1960).
[10]P. Maine, D Strickland, P. Bado *et. al,* IEEE J. Quantum Electron **24**, 2 (1988).
[11] E.L. Clark, K. Krushelnick, J.R. Davies *et. al*, Phys. Rev. Lett. **84**, 670 (2000).
[12] K. Cook, B.S. Thesis, (Houghton College, 2019).
[13] T. Kowalewski, B.S. Thesis, (Houghton College, 2021).
[14] J. Allison et al., Nucl. Instrum. Meth. A **835** 186-225 (2016).
[15] T. Sumikama, K. Matsuta, T. Nagatomo et. al, Phys. Rev. C **83**, 1-31 (2011).
[16] L. Weissman, C. Broude, G. Goldring *et. al* Nucl. Phys. A **630**, 678-688 (1998).
[17] A. J. Elwyn, R. E. Holland, C. N. Davids, and W. Ray, Jr., Phys. Rev. C **25**, 2168 (1982).
[18] B. W. Filippone, A. J. Elwyn, W. Ray, Jr., and D. D. Koetke, Phys. Rev. C **25**, 2174 (1982).
[19] A.E. Schilling, N.F. Mangelson, K.K. Nielson *et. al*, Nucl. Phys. A **263**, 389-396 (1976).
[20] C.R. McClenahan and Ralph E. Segel, Phys. Rev. C **11**, 370 (1975).
[21] R.W. Kavanagh, Nucl. Phys. **15**, 411-420 (1960).
[22] L. M. Baggett and S. J. Bame, Jr., Phys. Rev. **85,** 434 (1952).
[23] J.B. Woods and D.H. Wilkinson, Nucl. Phys. **61**, 661-674 (1965).
[24] S. Bashkin, Phys. Rev. **95**, 1012 (1954).
[25] N. Otuka, et al., Nuclear Data Sheets 120, 272-276 (2014).
[26] C. Freeman, G. Fiskel, C. Stoeckl *et. al* Rev. Sci. Instrum. **82**, 073301 (2011).
[27] M. Hatlo et al. Developments of Mathematical Software Libraries for the LHC experiments, IEEE Trans. Nucl. Sci. **52** (2005).
[28] R. Brun and F. Rademakers, ROOT - An Object Oriented Data Analysis Framework, Proceedings AIHENP'96 Workshop, Lausanne, Sep. 1996,
Nucl. Inst. & Meth. in Phys. Res. A **389** 81-86 (1997). See also "ROOT" [software], Release v6.24/06, 09/01/2021
[29] H. Chao, L. XiangQing, H. Hui *et. al* Sci. Sin-Phys. Mech. Astron. **42**, 10, 1056-1061 (2012).